Introduction of Cooperative Vehicle-to-Infrastructure Systems to Improve Speed Harmonization

PUBLICATION NO. FHWA-HRT-16-023

MARCH 2016

U.S. Department of Transportation
Federal Highway Administration

Research, Development, and Technology
Turner-Fairbank Highway Research Center
6300 Georgetown Pike
McLean, VA 22101-2296

FOREWORD

Cooperative vehicle-highway systems coordinate vehicle communications and remote traffic microwave sensors to increase overall system performance and sustainability. One strategy of cooperative vehicle-highway systems is speed harmonization, which dynamically adjusts vehicle speed recommendations in order to reduce speed differentials. This report describes a preliminary experiment of vehicle-to-infrastructure-based speed harmonization in which speed guidance is communicated directly to vehicles. This report reviews a set of micro-simulation experiments and a limited number of prototype field runs, including site selection, setup, and analysis. This report will be of interest to researchers concerned with implementation and utility of early cooperative vehicle-highway system deployments.

Paul Pisano
Acting Director, Office of Operations
Research and Development

TECHNICAL REPORT DOCUMENTATION PAGE

1. Report No. FHWA-HRT-16-023	2. Government Accession No.	3. Recipient's Catalog No.
4. Title and Subtitle Introduction of Cooperative Vehicle-to-Infrastructure Systems to Improve Speed Harmonization		5. Report Date March 2016 6. Performing Organization Code:
7. Author(s) David Hale, Thomas Phillips, Kelli Raboy, Jiaqi Ma, Patrick Su, Xiao-Yun Lu, Hesham Rakha, and Daniel J. Dailey		8. Performing Organization Report No.
9. Performing Organization Name and Address Leidos, Inc. 11251 Roger Bacon Drive Reston, VA 20190		10. Work Unit No. 11. Contract or Grant No. DTFH61-12-D-00020
12. Sponsoring Agency Name and Address Office of Operations Research and Development Federal Highway Administration 6300 Georgetown Pike McLean, VA 22101-2296		13. Type of Report and Period Covered Research Report 14. Sponsoring Agency Code HRDO-20

15. Supplementary Notes
The Contracting Officer's Representative was Joe Bared, HRDO-20.

16. Abstract
This project executed a preliminary experiment of vehicle-to-infrastructure (V2I)-based speed harmonization in which speed guidance was communicated directly to vehicles. This experiment involved a set of micro-simulation experiments and a limited number of prototype field runs. The simulation experiments produced mixed results in terms of system-wide benefits. The field runs demonstrated that connected and automated vehicles can successfully implement V2I-based speed harmonization and significantly reduce speed oscillations in their vicinity but do not have a significant impact on aggregate average speeds or travel times.

17. Key Words	18. Distribution Statement
Research, Connected vehicles, Automated vehicles, Speed harmonization, Field testing, Simulation	No restrictions. This document is available to the public through the National Technical Information Service, Springfield, VA 22161. http://www.ntis.gov

19. Security Classif. (of this report)	20. Security Classif. (of this page)	21. No. of Pages	22. Price
Unclassified	Unclassified	50	N/A

Form DOT F 1700.7 (8-72) Reproduction of completed page authorized.

SI* (MODERN METRIC) CONVERSION FACTORS

APPROXIMATE CONVERSIONS TO SI UNITS

Symbol	When You Know	Multiply By	To Find	Symbol
		LENGTH		
in	inches	25.4	millimeters	mm
ft	feet	0.305	meters	m
yd	yards	0.914	meters	m
mi	miles	1.61	kilometers	km
		AREA		
in^2	square inches	645.2	square millimeters	mm^2
ft^2	square feet	0.093	square meters	m^2
yd^2	square yard	0.836	square meters	m^2
ac	acres	0.405	hectares	ha
mi^2	square miles	2.59	square kilometers	km^2
		VOLUME		
fl oz	fluid ounces	29.57	milliliters	mL
gal	gallons	3.785	liters	L
ft^3	cubic feet	0.028	cubic meters	m^3
yd^3	cubic yards	0.765	cubic meters	m^3
	NOTE: volumes greater than 1000 L shall be shown in m^3			
		MASS		
oz	ounces	28.35	grams	g
lb	pounds	0.454	kilograms	kg
T	short tons (2000 lb)	0.907	megagrams (or "metric ton")	Mg (or "t")
		TEMPERATURE (exact degrees)		
^oF	Fahrenheit	5 (F-32)/9 or (F-32)/1.8	Celsius	^oC
		ILLUMINATION		
fc	foot-candles	10.76	lux	lx
fl	foot-Lamberts	3.426	$candela/m^2$	cd/m^2
		FORCE and PRESSURE or STRESS		
lbf	poundforce	4.45	newtons	N
lbf/in^2	poundforce per square inch	6.89	kilopascals	kPa

APPROXIMATE CONVERSIONS FROM SI UNITS

Symbol	When You Know	Multiply By	To Find	Symbol
		LENGTH		
mm	millimeters	0.039	inches	in
m	meters	3.28	feet	ft
m	meters	1.09	yards	yd
km	kilometers	0.621	miles	mi
		AREA		
mm^2	square millimeters	0.0016	square inches	in^2
m^2	square meters	10.764	square feet	ft^2
m^2	square meters	1.195	square yards	yd^2
ha	hectares	2.47	acres	ac
km^2	square kilometers	0.386	square miles	mi^2
		VOLUME		
mL	milliliters	0.034	fluid ounces	fl oz
L	liters	0.264	gallons	gal
m^3	cubic meters	35.314	cubic feet	ft^3
m^3	cubic meters	1.307	cubic yards	yd^3
		MASS		
g	grams	0.035	ounces	oz
kg	kilograms	2.202	pounds	lb
Mg (or "t")	megagrams (or "metric ton")	1.103	short tons (2000 lb)	T
		TEMPERATURE (exact degrees)		
^oC	Celsius	1.8C+32	Fahrenheit	^oF
		ILLUMINATION		
lx	lux	0.0929	foot-candles	fc
cd/m^2	$candela/m^2$	0.2919	foot-Lamberts	fl
		FORCE and PRESSURE or STRESS		
N	newtons	0.225	poundforce	lbf
kPa	kilopascals	0.145	poundforce per square inch	lbf/in^2

*SI is the symbol for the International System of Units. Appropriate rounding should be made to comply with Section 4 of ASTM E380.
(Revised March 2003)

TABLE OF CONTENTS

EXECUTIVE SUMMARY **1**
SITE SELECTION **1**
RESEARCH RESULTS **4**
NEXT STEPS **4**
CHAPTER 1. SIMULATION EXPERIMENTS **5**
SPEED-BASED ALGORITHM **5**
Description 5
Testing 7
DENSITY-BASED ALGORITHM **9**
Description 9
Testing (Part 1: INTEGRATION© Platform) 17
Testing (Part 2: VISSIM® Platform) 19
CHAPTER 2. FIELD EXPERIMENTS **23**
VEHICLE AND INFRASTRUCTURE SETUP **23**
Vehicles 23
Infrastructure 23
METHODOLOGY **25**
ANALYSIS **27**
Vehicle Control 28
Probe Vehicles/Sensors 28
Potential Benefits 35
CHAPTER 3. CONCLUSIONS **37**
ACKNOWLDGEMENTS **39**
REFERENCES **41**

LIST OF FIGURES

Figure 1. Map. Geographic scope of the study area and typical traffic situation in afternoon peak hours 2
Figure 2. Graph. I-66 probe vehicle actual and average speed trajectories 3
Figure 3. Graph. I-66 probe vehicle actual and average speed trajectories with harmonic model 3
Figure 4. Equation. Speed-based algorithm speed advisory in bottleneck 5
Figure 5. Equation. Speed-based algorithm speed advisory upstream of bottleneck 5
Figure 6. Equation. Speed-based algorithm minimum group speed approach 6
Figure 7. Equation. Speed-based algorithm average group speed approach 7
Figure 8. Equation. Speed-based algorithm TTT adjustment 8
Figure 9. Equation. Speed-based algorithm TD adjustment 8
Figure 10. Equation. Speed-based algorithm TNOS adjustment 8
Figure 11. Illustration. Lane-drop bottleneck 10
Figure 12. Equation. Steady-state flow as a function of density 10
Figure 13. Equation. Steady-state speed as a function of density 10
Figure 14. Illustration. Fundamental diagram of traffic flow 11
Figure 15. Equation. Mathematical formulation of the density-based algorithm 12
Figure 16. Equation. Estimation of flow rates 12
Figure 17. Equation. Steady-state density as a reverse function of speed 13
Figure 18. Equation. Steady-state density as a reverse function of flow 13
Figure 19. Flowchart. Density-based algorithm logic and advisory speed recommendations 14
Figure 20. Equation. Density-based algorithm step 1—advisory speed recommendation 15
Figure 21. Equation. Density-based algorithm step 1—optimal flow rate 15
Figure 22. Equation. Density-based algorithm step 2—flow and density conditions 15
Figure 23. Equation. Density-based algorithm step 2—time lag 15
Figure 24. Equation. Density-based algorithm step 2—advisory speed recommendation 1 15
Figure 25. Equation. Density-based algorithm step 2—target flow rate 1 16
Figure 26. Equation. Density-based algorithm step 2—target flow rate 2 16
Figure 27. Equation. Density-based algorithm step 2—advisory speed recommendation 2 16
Figure 28. Equation. Density-based algorithm step 3—advisory speed recommendation 1 16
Figure 29. Equation. Density-based algorithm step 3—advisory speed recommendation 2 16
Figure 30. Equation. Density-based algorithm step 3—target flow rate 16
Figure 31. Graph. Vehicle trajectories before and after applying the density-based algorithm in INTEGRATION© 19
Figure 32. Map. Field experiment map of system integration 24
Figure 33. Map. Test segment and trailer locations 24
Figure 34. Illustration. Research and probe vehicle placement 26
Figure 35. Equation. Field experiment speed recommendation 27
Figure 36. Graph. Control vehicle trajectories and recommendations 28
Figure 37. Graph. Temporal speed trajectories 29
Figure 38. Graph. Spatial speed trajectories 29
Figure 39. Graph. Control speed trajectory and smoothed profile 30
Figure 40. Graph. Detrended probe vehicle speed trajectories 31
Figure 41. Graph. PDF of raw data following probe speed trajectory 32

Figure 42. Graph. PDF of detrended following probe speed trajectory.....32
Figure 43. Graph. PDF of detrended leading probe speed trajectory 33
Figure 44. Graph. PSDs of detrended speed trajectories of the probe vehicles on July 8, 2014.....34
Figure 45. Graph. PSDs of detrended speed trajectories of the probe vehicles on September 29, 2015 34
Figure 46. Graph. PSDs of detrended speed trajectories of the probe vehicles on October 15, 2015.....35
Figure 47. Graph. PSDs of detrended speed trajectories of the probe vehicles on October 21, 2015.....35

LIST OF TABLES

Table 1. System performance impacts of the speed-based algorithm in Aimsun® 9
Table 2. Speed harmonization algorithm settings 18
Table 3. Density-based algorithm simulation results in INTEGRATION© with limited research vehicles 18
Table 4. Operational MOEs in VISSIM® (three-car case) 20
Table 5. Safety surrogate MOEs in VISSIM® (three-car case) 20
Table 6. Travel times at various market penetration rates in VISSIM® 21
Table 7. Speeds at various market penetration rates in VISSIM® 21
Table 8. Throughput at various market penetration rates in VISSIM® 21
Table 9. Stops at various market penetration rates in VISSIM® 21
Table 10. Lane changes at various market penetration rates in VISSIM® 21
Table 11. Cumulative speed difference at various market penetration rates in VISSIM® 22

LIST OF ABBREVIATIONS

ACC	adaptive cruise control
CO_2	carbon dioxide
CO	carbon monoxide
CMTS	connected mobile traffic sensing
CAV	connected and automated vehicle
HC	hydrocarbons
LHS	Latin hypercube sampling
LTM	log transformation method
MOE	measures of effectiveness
NOx	nitrogen oxides
OEM	original equipment manufacturer
OD	origin-destination
PSD	power spectral density
PDF	probability density function
RMSE	root mean square error
RTMS	remote traffic microwave sensor
TD	total delay
TNOS	total number of stops
TTD	total travel distance
TTT	total travel time
TFHRC	Turner-Fairbank Highway Research Center
V2I	vehicle-to-infrastructure

EXECUTIVE SUMMARY

The U.S. Department of Transportation's Federal Highway Administration has initiated a research program on cooperative vehicle-to-infrastructure (V2I) highway systems with the goal of increasing overall system performance and sustainability, including safety, mobility, and environmental impacts. Cooperative vehicle-highway systems coordinate vehicle communications and remote traffic microwave sensors (RTMSs) in pursuit of these goals. One strategy of cooperative vehicle-highway systems is speed harmonization, which dynamically adjusts vehicle speed recommendations in order to reduce speed differentials. Speed harmonization can be applied near areas of congestion, accidents, or special events to optimize mobility and safety. Speed harmonization has been implemented in a few locations in the United States with some success, but the current approach faces significant challenges. As presently implemented, speed harmonization is conducted with the use of variable speed limit signs or dynamic message signs. This method of implementation is susceptible to unpredictable and uncoordinated driver response. Moreover, these signs are costly for State and local agencies to deploy, operate, and maintain.

Despite these challenges, simulation has shown that speed harmonization does not require perfect driver compliance to significantly improving traffic flow and performance.[1,2] In this project, researchers performed a preliminary experiment of V2I-based speed harmonization in which speed guidance was communicated directly to vehicles. This experiment involved a set of micro-simulation experiments and a limited number of prototype field runs.

SITE SELECTION

Speed harmonization is believed to produce significant benefits at sites where excessive vehicle speed oscillations cause premature formation of congestion and bottlenecks. The section of I-66 inside the beltway (I-495) approaching Washington, DC, is a congested roadway with one of the least dependable travel times in the United States.[3] Daily recurring congestion at the merge of VA-267 into I-66 (and the subsequent lane drops) leads to a "stop-and-go" formation. At this site, shown in figure 1, it was hypothesized that speed harmonization could have a positive impact.

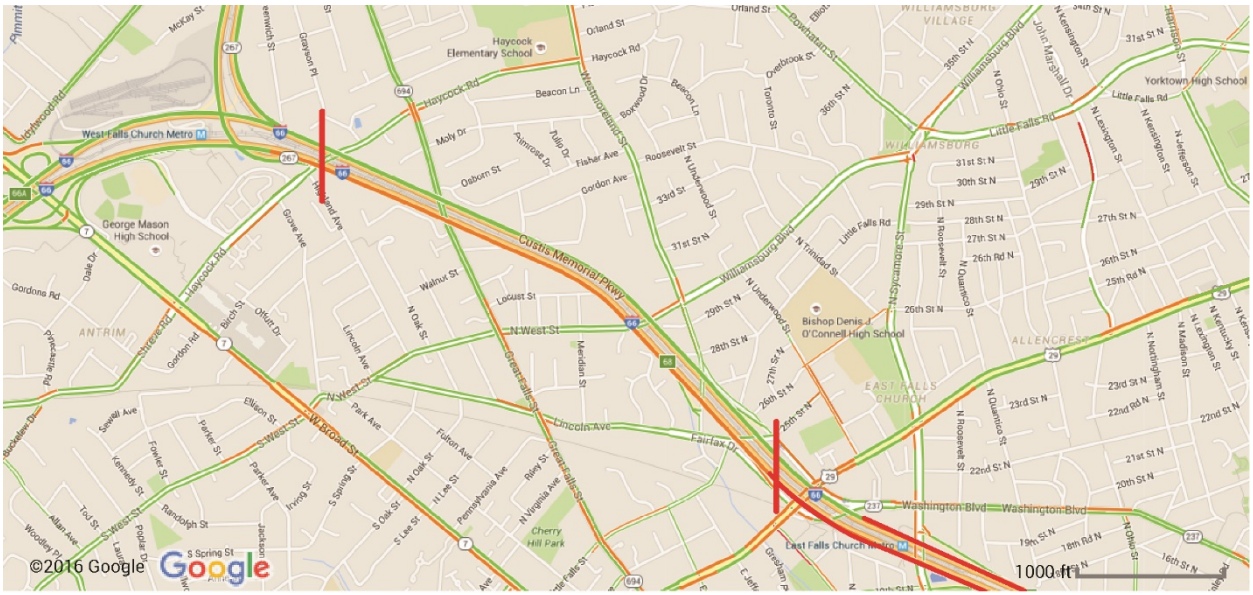

©2016 Google®

Figure 1. Map. Geographic scope of the study area and typical traffic situation in afternoon peak hours.(4)

In order to understand the traffic dynamics on this section of freeway, a number of field runs were used to identify typical speed trajectories during weekday peak periods. These field runs were performed by probe vehicles equipped with Global Positioning System receivers, cell phones, and computers. The computers transmitted vehicle trajectories in real time to servers at the Saxton Transportation Operations Laboratory in McLean, VA. Trajectories were transmitted before and during the recurring congested period. Figure 2 illustrates actual probe speed trajectories shown in blue plus a computed average trajectory shown in red. The average trajectory shows a significantly trended periodic component. Large features of the average trajectory can be described by a sinusoid, as shown in figure 3. The oscillatory trend shown in figure 3 will increase fuel consumption and may impact mobility and safety. Given this recurring structure in the speed profiles along I-66, the corridor was deemed a suitable candidate for the experiment on speed harmonization using connected and automated vehicles (CAVs).

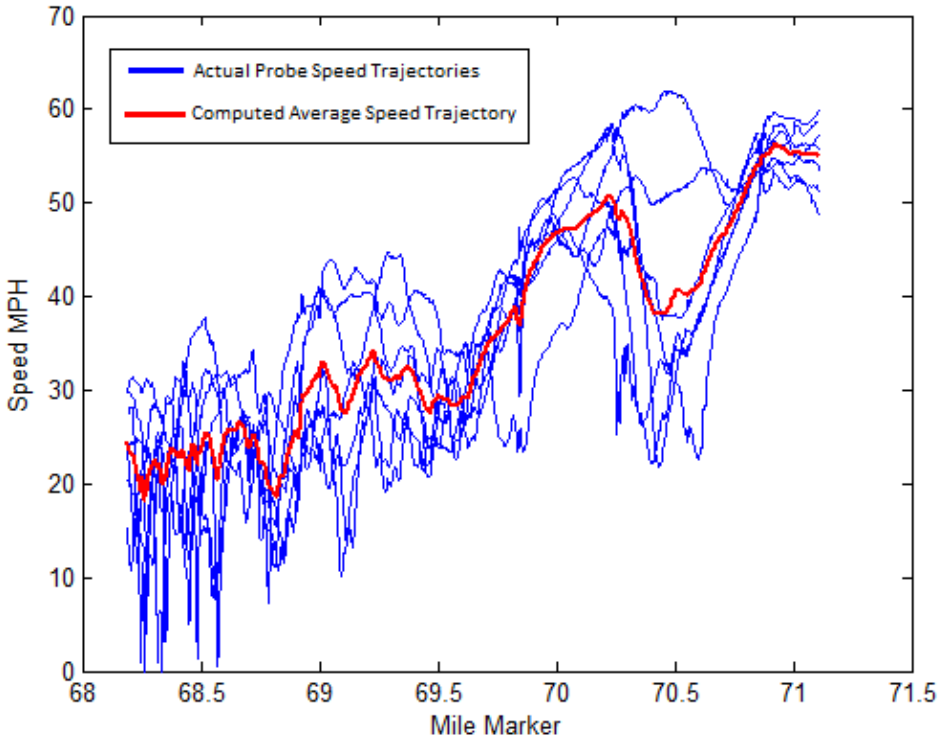

1 mi/h = 1.61 km/h

Figure 2. Graph. I-66 probe vehicle actual and average speed trajectories.

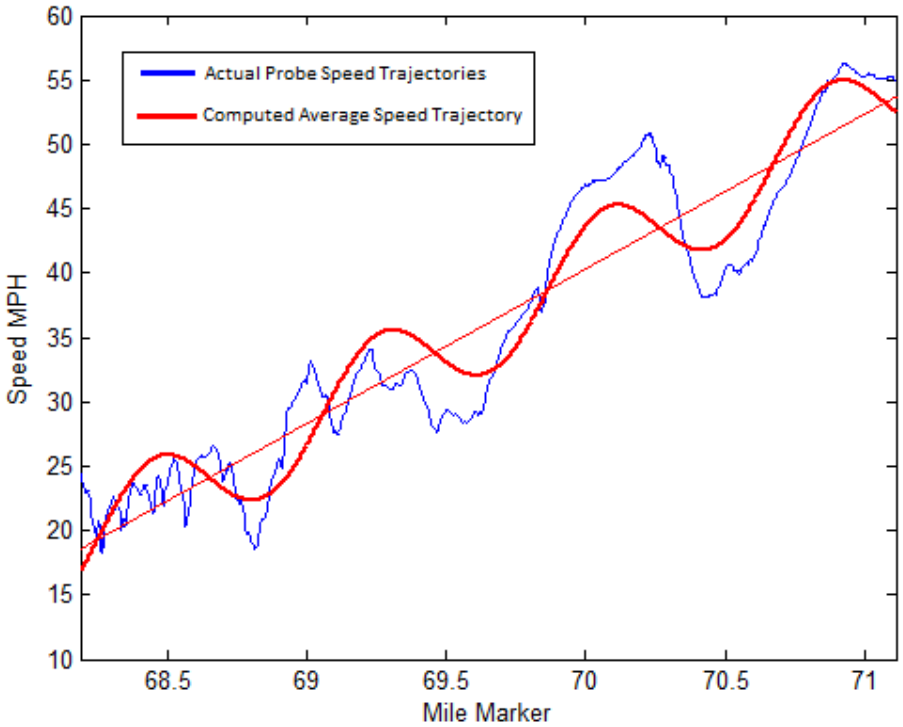

1 mi/h = 1.61 km/h

Figure 3. Graph. I-66 probe vehicle actual and average speed trajectories with harmonic model.

RESEARCH RESULTS

Due to resource constraints, the field experiments could only deploy a maximum of three CAVs. Simulation results across three software platforms (VISSIM®, INTEGRATION©, and Aimsun®) showed that the introduction of three CAVs, with a goal of harmonizing overall speeds, did not produce macroscopic traffic benefits.[5–7] When analyzing higher CAV penetration rates, the simulation experiments produced mixed results.

On the Aimsun® platform, all penetration rates above 10 percent produced corridor-wide travel time reductions between 8 and 10 percent. The researchers concluded that this was due to congested conditions that minimized lane changing (i.e., if 10 percent of vehicles reduced their speeds, most other vehicles were impacted). Similar results were observed on the INTEGRATION© platform, where all penetration rates above 10 percent produced corridor-wide delay reductions between 7 and 11 percent. On the VISSIM® platform, a 1,000-ft (300-m) freeway segment believed to be most impacted by speed harmonization saw 32, 39, and 42 percent travel time reductions under penetration rates of 10, 25, and 50 percent, respectively. However, corridor-wide travel time reductions were only 1, 2, and 3 percent, respectively.

Although the simulation experiments produced mixed results, the results were positive enough to warrant follow-up field experiments. These experiments demonstrated that with modifications to the manufacturer-supplied adaptive cruise control (ACC), CAVs can successfully implement V2I-based speed harmonization, at least from a mechanical standpoint. From an operational standpoint, the field experiments were constrained by the availability of only three CAVs. These vehicles were shown to significantly reduce speed oscillations in their vicinity but did not have a significant impact on aggregate average speeds or travel times, which is consistent with the simulation outcomes.

NEXT STEPS

Future field experiments should thus include a larger number of CAVs. Future algorithm development should optimize vehicle speeds to achieve maximum safety benefits. If a bottleneck is not yet formed, slowing the right proportion of vehicles could prevent or delay the onset of bottleneck formation. If a bottleneck is already formed, slowing all vehicles by the right amount could mitigate bottleneck severity. Other factors subject to optimization include CAV penetration rates, speed reduction magnitudes, and lane-specific congestion levels. The remainder of this report summarizes the technical details from phase 1 of the V2I-based speed harmonization research.

CHAPTER 1. SIMULATION EXPERIMENTS

Prior to the field runs, speed harmonization algorithms were analyzed in micro-simulation environments. The simulation experiments examined various levels of CAV market penetration. Two speed harmonization algorithms were tested: speed-based and density-based. The speed-based algorithm was tested using Aimsun®, and the density-based algorithm was tested using INTEGRATION© and VISSIM®.

SPEED-BASED ALGORITHM

Description

The speed-based algorithm determines advisory speeds for freeway segments upstream and downstream of a known bottleneck location based on measured speeds within the bottleneck area. The speed-based algorithm is intended to increase throughput and prevent bottleneck formation.

Within a bottleneck area, the speed-based algorithm tends to generate advisory speeds 10 to 50 percent higher than measured bottleneck speeds (see figure 4). Although the algorithm looks very simple, its function realizes the control philosophy in previous work.[8] This approach does not claim system optimization yet emphasizes simplicity and practical field implementation.

$$u_m(k) = \alpha_m \times \bar{v}_m(k)$$

Figure 4. Equation. Speed-based algorithm speed advisory in bottleneck.

Where:

$u_m(k)$ = Variable speed advisory at time step k in section m.
α_m = Proportional control gain in section m, where $\alpha_m \in [1.1, 1.5]$; default value: $\alpha_m = 1.3$.
$\bar{v}_m(k)$ = Measured speed of the bottleneck.

Upstream of a bottleneck area, when traffic congestion approaches capacity levels, the speed-based algorithm tends to generate advisory speeds 10 to 30 percent below measured bottleneck speeds (see figure 5). Figure 5 shows that when bottleneck speed decreases, upstream advisory speed is proportionally reduced. This is equivalent to reducing flow to the bottleneck. When bottleneck speed increases, upstream advisory speed is proportionally increased. This increases bottleneck throughput towards its capacity.

$$u_{m+1}(k) = \begin{cases} V_{free}, & \text{if } \bar{o}_m(k) < O_{sw} \\ \beta_m \times \bar{v}_m(k), & \text{if } \bar{o}_m(k) \geq O_{sw} \end{cases}$$

Figure 5. Equation. Speed-based algorithm speed advisory upstream of bottleneck.

Where:

$u_{m+1}(k)$ = Variable speed advisory at time step k in section $m + 1$.
V_{free} = Free-flow speed.
$\bar{o}_m(k)$ = Measured occupancy in bottleneck section.

O_{sw} = Switch threshold of occupancy close to the capacity flow (suggested value is between 10.0 and 12.5 percent).
β_m = Proportional control gain in section m, where $\beta_m \in [0.7, 0.9]$; default value: $\beta_m = 0.8$.

The speed-based speed harmonization algorithm streamlines traffic flow on each freeway segment. When there are multiple bottlenecks on a segment, advisory speeds for the segments between bottlenecks can be determined by distance-based interpolation.

To implement the advisory speeds for each freeway segment, CAVs are assumed to be discharged in platoons. The objective is for these vehicles to drive in parallel at the same speed on adjacent lanes in order to block all upstream vehicles. This forces all following vehicles to comply with the advisory speed.

Due to large variations in driver behavior on I-66, traffic speeds cannot be considered homogenous in both time and space. As a result, CAVs could use advisory speeds as set speeds but may not be able to drive at those speeds. Moreover, there would be speed differences between these CAVs on different lanes. When blocked by other vehicles in slow lanes, CAVs are expected to lag behind. Such situations have been observed in simulation. Therefore, it is necessary to adjust advisory speeds according to CAV speeds at a microscopic level. The following describes two methods of speed fusion tested through simulation: minimum group speed and average group speed.

Minimum Group Speed

Figure 6 implements an approach that uses the minimum speed of a group of research vehicles (i.e., the minimum group speed approach). First, the minimum speed among a group of CAVs is selected using lead vehicle speed in each lane. Then for each group and section that the group currently resides in, minimum speed is fused with global advisory speed (see figure 6). In essence, this fusion approach (based on market penetration rates) dictates that all CAVs must drive either at a similar speed or side-by-side.

$$u_{i,m}^{des}(k) = \begin{cases} u_m(k), & V_i^{\min}(k) \geq 50 \\ 0.3V_i^{\min}(k) + 0.7u_m(k), & 40 \leq V_i^{\min}(k) \leq 50 \\ 0.5V_i^{\min}(k) + 0.5u_m(k), & 30 \leq V_i^{\min}(k) \leq 40 \\ 0.7V_i^{\min}(k) + 0.3u_m(k), & 15 \leq V_i^{\min}(k) \leq 30 \\ 0.85V_i^{\min}(k) + 0.15u_m(k) & V_i^{\min}(k) \leq 15 \end{cases}$$

Figure 6. Equation. Speed-based algorithm minimum group speed approach.

Where:

$u_{i,m}^{des}(k)$ = Variable speed advisory at time step k in section m for a typical group i of CAVs.
$V_i^{min}(k)$ = Minimum measured speed at time step k for a typical group i of CAVs.

Average Group Speed

Figure 7 implements an approach that uses the average speed of a group of research vehicles (i.e., the average group speed approach). First, the average speed among a group of CAVs is estimated. If there is more than one vehicle in each lane, this is accomplished by selecting the average speed among leader vehicles in each lane. Then for each group and each section that the group currently resides in, average speed is fused with global advisory speed (see figure 7). In contrast with the minimum group speed approach, the average group speed approach dictates that CAVs do not need to drive side-by-side. They are allowed to have more speed differential within the same group but retain a close proximity, as determined by the weighting factors.

$$u_{i,m}^{des}(k)=\begin{cases} u_m(k), & V_i^{ave}(k)\geq 50 \\ 0.3V_i^{ave}(k)+0.7u_m(k), & 40\leq V_i^{ave}(k)\leq 50 \\ 0.5V_i^{ave}(k)+0.5u_m(k), & 30\leq V_i^{ave}(k)\leq 40 \\ 0.7V_i^{ave}(k)+0.3u_m(k), & 15\leq V_i^{ave}(k)\leq 30 \\ 0.85V_i^{ave}(k)+0.15u_m(k) & V_i^{ave}(k)\leq 15 \end{cases}$$

Figure 7. Equation. Speed-based algorithm average group speed approach.

Where:

$V_i^{ave}(k)$ = Average measured speed at time step k for a typical group i of CAVs.

Testing

The speed-based algorithm was tested on the Aimsun® simulation platform. The results are presented in the following subsections.

Calibration

Most default values for parameters such as time headway distribution and variance, maximum acceleration and variation, etc., were obtained from Performance Measurement System and Next Generation SIMulation data analyses. Two performance parameters were used to quantify the discrepancy between field-measured and simulated results in terms of throughput: relative root mean square error (RMSE) and the GEH statistic. Throughput comparisons were performed at all freeway mainline sensors, and speed comparisons were performed at three sensors.

An iterative calibration process was used. This process included progressive calibration at each sensor location from downstream to upstream and then in the reverse direction. This progressive calibration was necessary because upstream and downstream flows and speeds affect each other. The objective was to match both flows and time-mean speeds at fixed sensor locations. Minor demand adjustments were made to correct some sensor measurement errors, which were usually about 5 to 10 percent in practice. Engineering judgment was used to perform trial-and-error adjustments of both flows and speeds for upstream and downstream traffic situations. To obtain unbiased (i.e., “apples-to-apples”) comparisons, it was important to confirm that all demand volumes were discharged at the end of each simulation run.

Analysis

The proposed speed-based algorithm was simulated using the calibrated Aimsun® network for 3 virtual days with compliance rates of 10, 25, 50, and 100 percent. Each date was simulated for 10 replications (random number seeds) to get their mean. The following macroscopic performance measures were used to evaluate the algorithms' implementations within simulation: total travel time (TTT), total travel distance (TTD), total delay (TD) (obtained by deducting hypothetical free-flow travel times from simulated travel times), speed variation (directly reflects fluctuations in system-wide speed), total number of stops (TNOS) (used as a system-wide performance parameter for traffic smoothness in Aimsun®), and outflow (throughput) changes at bottlenecks.

CAV groups were regularly dispatched into the freeway segment from upstream of the I-66 and VA-267 merge. All CAVs were in ACC mode with fused speeds as set speeds, and all other vehicles were in human driver mode. Dispatching time intervals of 60, 90, 120, 900, and 1,800 s were used in simulation. In addition to the speed harmonization set speed, two other factors affected the practical speeds: downstream traffic and the speed of other vehicles in the group. Each lane had at least one CAV lane controlled through the Aimsun® application program interface.

Since the simulation model was set during the afternoon peak hours between 3 and 9 p.m., different random number seeds produced different demand flow patterns (from entrance ramp and freeway mainline), resulting in slightly different total (cumulative) demands. Higher total demands within any simulation time interval could result in longer TTT even if the speed harmonization algorithm was functioning properly. To overcome this bias, the following adjustments shown in figure 8 through figure 10 were applied when estimating percentage time improvements for TTT, TD, and TNOS. For example, if TTD increased by 10 percent after simulation, then TTT and TD were decreased by 10 percent as a penalty. Here the subscripts indicate whether parameters were estimated from the default scenario (default) or from data with speed control activated (vsa).

$$TTT\%Change = \frac{TTT_{default} - TTT_{vsa}}{TTT_{default}} - \frac{TTD_{default} - TTD_{vsa}}{TTD_{default}}$$

Figure 8. Equation. Speed-based algorithm TTT adjustment.

$$TD\%Change = \frac{TD_{default} - TD_{vsa}}{TD_{default}} - \frac{TTD_{default} - TTD_{vsa}}{TTD_{default}}$$

Figure 9. Equation. Speed-based algorithm TD adjustment.

$$TNOS\%Change = \frac{TNOS_{default} - TNOS_{vsa}}{TNOS_{default}} - \frac{TTD_{default} - TTD_{vsa}}{TTD_{default}}$$

Figure 10. Equation. Speed-based algorithm TNOS adjustment.

Table 1 shows that the system-wide performance measures when using the average group speed approach improved under faster dispatch rates. In a real-world field test, the fastest dispatching

rates would be constrained by the total number of CAVs available and the time needed to finish a run cycle.

Table 1. System performance impacts of the speed-based algorithm in Aimsun®.

CAV Dispatch Rate (s)	TTT (Percent)	TTD (Percent)	TD (Percent)	Speed Variation (Percent)	Average Number of Stops (Percent)	Flow Downstream of Bottleneck (Percent)	Flow at Bottleneck (Percent)
1,800	-0.63	-0.04	-1.84	0.19	0.070	-0.18	-0.41
900	-1.54	-0.03	-3.46	-0.17	0.180	0.01	-0.31
120	-4.08	0.52	-7.09	-0.97	0.013	0.49	-0.39
90	-4.45	0.66	-5.82	-1.01	-0.230	0.42	-0.57
60	-6.53	0.87	-9.14	-1.94	0.190	0.67	-0.65

DENSITY-BASED ALGORITHM

Description

The objective of the density-based algorithm is to prevent upstream density from exceeding a critical density. The algorithm also tries to maximize bottleneck throughput by metering upstream flows. The algorithm searches for an optimal density that can maximize the bottleneck discharge rates while eliminating capacity drops. In the density-based algorithm, this optimal density is called the "target density."

Figure 11 illustrates a lane-drop bottleneck. The road section is divided into three zones: the speed harmonization zone, the acceleration zone, and the bottleneck. In order to develop a speed harmonization algorithm, three sets of sensors are placed: one in the speed harmonization zone, one directly upstream of the bottleneck, and one directly downstream of the bottleneck. If on- and/or off-ramps exist between the speed harmonization zone and the bottleneck, sensors are needed on the on- and off-ramps to record traffic flow. Sensors gather volume, speed, and occupancy data for use in the algorithm. CAVs in the speed harmonization zone receive advisory speed recommendations from a traffic management center to control flow arriving at the bottleneck.

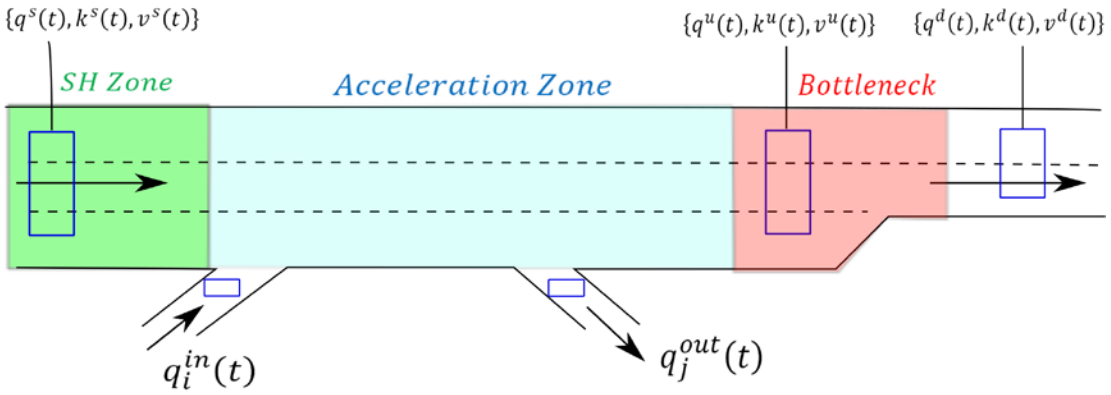

Figure 11. Illustration. Lane-drop bottleneck.

Where:

SH Zone = Speed harmonization zone.
$q^s(t)$ = Flow rate in the speed harmonization zone at time *t*.
$k^s(t)$ = Density of the speed harmonization zone at time *t*.
$v^s(t)$ = Speed in the speed harmonization zone at time *t*.
$q_i^{in}(t)$ = On-ramp flow rate at time *t*.
$q_i^{out}(t)$ = Off-ramp flow at time *t*.
$q^u(t)$ = Capacity of the bottleneck zone at time *t*.
$k^u(t)$ = Density at capacity of the bottleneck zone at time *t*.
$v^u(t)$ = Speed in the bottleneck zone at time *t*.
$q^d(t)$ = Downstream capacity of the bottleneck at time *t*.
$k^d(t)$ = Downstream density at capacity of the bottleneck at time *t*.
$v^d(t)$ = Speed downstream of the bottleneck at time *t*.

The speed harmonization approach assumes that a steady-state fundamental diagram exists to relate the traffic stream flow (q), density (k), and speed (v) given the functions in figure 12 and figure 13.

$$q = Q(k)$$

Figure 12. Equation. Steady-state flow as a function of density.

Where:

$Q(k)$ = General function Q of k based on a calibrated fundamental diagram.

$$v = V(k)$$

Figure 13. Equation. Steady-state speed as a function of density.

Where:

$V(k)$ = General function V of k based on a calibrated fundamental diagram.

Figure 14 shows the fundamental diagram for upstream and downstream sections of the bottleneck.

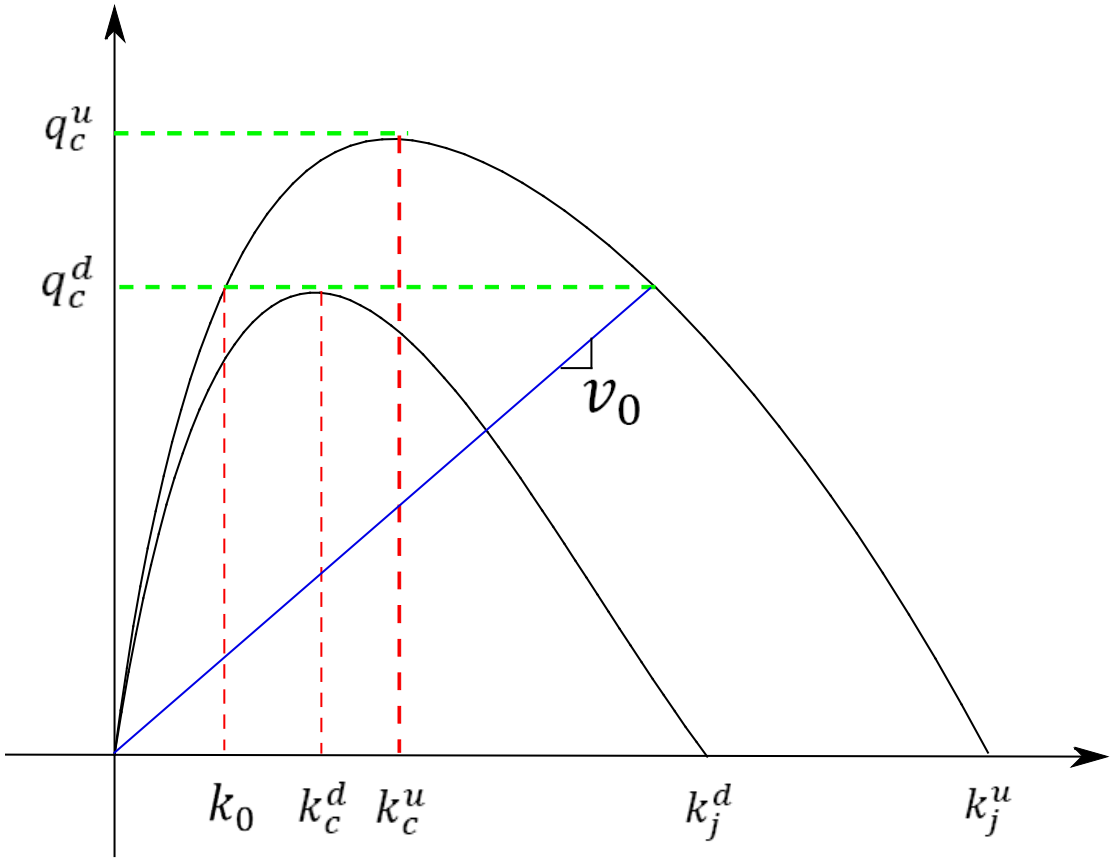

Figure 14. Illustration. Fundamental diagram of traffic flow.

Where:

q_c^u = Capacity directly upstream of the bottleneck.
q_c^d = Downstream capacity of the bottleneck.
v_0 = Advisory speed recommendation.
k_c^d = Downstream density at capacity of the bottleneck.
k_c^u = Density at capacity directly upstream of the bottleneck.
k_j^d = Downstream jam density of the bottleneck.
k_j^u = Jam density directly upstream of the bottleneck.

In order to avoid a traffic breakdown upstream of the bottleneck, arrivals are constrained at the bottleneck. Here, target density k_0 (or its equivalent occupancy given that density cannot be measured in the field) is set in order to achieve the desired objective. The in-flow rate of the bottleneck at the capacity of the bottleneck is controlled.

The primary objective function of the speed harmonization algorithm is to maximize a weighted combination of flow downstream of the bottleneck and to minimize speed variability within the speed harmonization section, as shown in figure 15.

$$\max_{v_0(t)} \sum_{t=1}^{T} \left(w_q q^d(t) + \frac{w_v}{\tilde{v}^s(t)} \right)$$

Subject to:

$$k^u(t) \leq k_c^u;$$
$$\hat{q}^s(t) \leq q_c^d + q_r(t);$$
$$\Delta v(t) \leq \Delta v_{thr};$$
$$\tilde{v}_0(t) \geq v_{min}$$

Figure 15. Equation. Mathematical formulation of the density-based algorithm.

Where:

$v_0(t)$ = Set of all possible advisory speed recommendations in the speed harmonization zone at time *t*.
T = Total simulation time.
w_q = Weight assigned to the flow directly downstream of the bottleneck.
w_v = Weight assigned to the speed variability in the speed harmonization zone.
$\tilde{v}^s(t)$ = Measure of speed variability in the speed harmonization zone (i.e., the standard deviation of the speed in the speed harmonization zone at the control duration).
$\hat{q}^s(t)$ = Flow rate at time *t* in speed harmonization zone.
$q_r(t)$ = Sum of flow rates at all on- and off-ramps between the speed harmonization zone and the bottleneck at instant *t*.
$\Delta v(t)$ = Difference between speed advisory speed recommendations over the control interval in the speed harmonization zone at time *t*.
Δv_{thr} = Maximum allowed change in control speed in the speed harmonization zone.
$\tilde{v}_0(t)$ = Advisory speed recommendation in the speed harmonization zone at time *t*.
v_{min} = Minimum advisory speed recommendation.

One criterion to determine when the speed harmonization should be activated can be expressed as $k_c^u = k_0$. Also, $q_r(t)$ can be estimated using figure 16.

$$q_r(t) = \sum q_j^{out}\left(t + l_j^{out}\right) - \sum_i q_i^{in}\left(t + l_i^{in}\right)$$

Figure 16. Equation. Estimation of flow rates.

Where:

l_j^{out} = Lag for vehicles traveling from speed harmonization zone to off-ramp *j*.
l_j^{in} = Lag from speed harmonization zone to on-ramp *i*.

Lags are computed assuming that vehicles travel from the speed harmonization zone to given locations at the free-flow speed or, potentially, at the prevailing space-mean speed. In that sense, some form of prediction is needed to predict these flows.

$\tilde{v}_0(t)$ can be estimated to achieve optimal flow rates in the speed harmonization zone, $\tilde{q}_0(t)$. Reverse functions for flow-density and speed-density relationships under congested traffic can be defined to reflect the area upstream of the bottleneck as follows:

$$k = V^{-1}(v),\ k_c^u \le k < k_j^u$$

Figure 17. Equation. Steady-state density as a reverse function of speed.

$$k = Q^{-1}(q),\ k_c^u \le k < k_j^u$$

Figure 18. Equation. Steady-state density as a reverse function of flow.

Figure 19 illustrates a flowchart of the algorithm, which is described in the succeeding list.

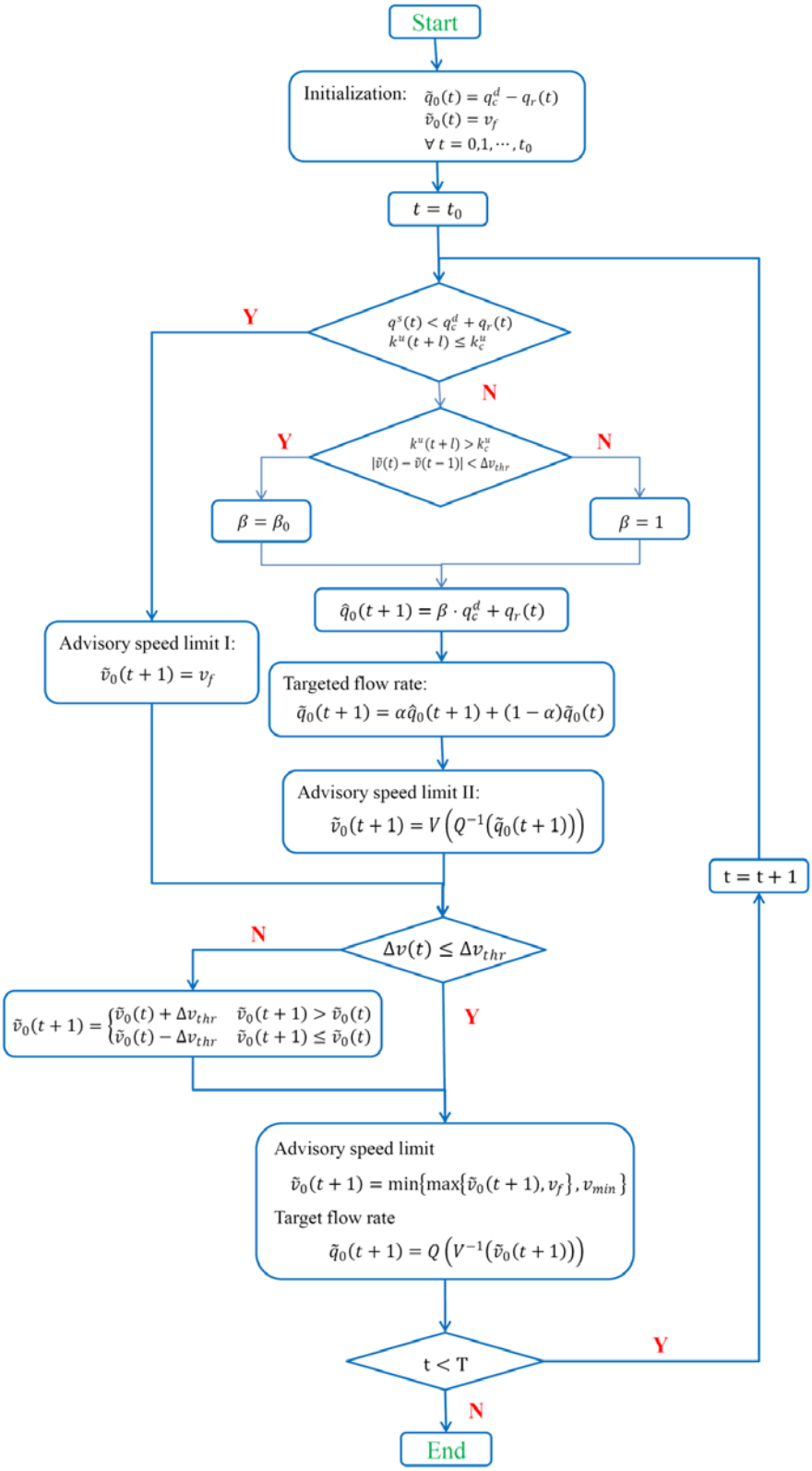

Figure 19. Flowchart. Density-based algorithm logic and advisory speed recommendations.

1. When $t \leq t_0$ (starting time when the algorithm is activated), assign the speed harmonization zone advisory speed recommendation, as shown in figure 20.

$$\tilde{v}_0(t) = v_f$$

Figure 20. Equation. Density-based algorithm step 1—advisory speed recommendation.

Where:

v_f = Free flow speed.

Optimal flow rate in the speed harmonization zone is set, as shown in figure 21.

$$\tilde{q}_0(t) = q_c^d + q_r(t)$$

Figure 21. Equation. Density-based algorithm step 1—optimal flow rate.

2. At each time step *t*, check the two conditions, as shown in figure 22.

$$\begin{cases} q^s(t) < q_c^d + q_r(t) \\ k^u(t+1) \leq k_c^u \end{cases}$$

Figure 22. Equation. Density-based algorithm step 2—flow and density conditions.

Where:

l = Time lag for vehicles traveling from speed harmonization zone to bottleneck (see figure 23).

$$l = \frac{L}{v_l}$$

Figure 23. Equation. Density-based algorithm step 2—time lag.

Where:

L = Distance from speed harmonization zone to bottleneck.
v_l = Either the free-flow or space-mean speed of prevailing traffic streams.

If both conditions are satisfied, set the advisory speed recommendation, as shown in figure 24.

$$\tilde{v}_0(t+1) = v_f$$

Figure 24. Equation. Density-based algorithm step 2—advisory speed recommendation 1.

If either one of the conditions is violated, first compute a target flow rate in the speed harmonization zone, as shown in figure 25.

$$\hat{q}_0(t+1) = \beta \times q_c^d + q_r(t)$$

Figure 25. Equation. Density-based algorithm step 2—target flow rate 1.

Where:

β = Coefficient for bottleneck capacity.

If $k^u(t+l) > k_c^u$ and $|\tilde{v}(t) - \tilde{v}(t-1)| < \Delta v_{thr}$, set $\beta = \beta_0$.

Where:

β_0 = Coefficient of bottleneck capacity.

If $\beta_0 < 1$, then, $\beta \times q_c^d$ is less than the maximum bottleneck discharge flow rate when capacity drops happen. Otherwise, let $\beta = 1$.

Target flow rate is computed in the next time step, as shown in figure 26.

$$\tilde{q}_0(t+1) = \alpha\hat{q}_0(t+1) + (1-\alpha)\tilde{q}_0(t)$$

Figure 26. Equation. Density-based algorithm step 2—target flow rate 2.

Where:

α = Smoothing factor.

An advisory speed recommendation is made at $t + 1$, as shown in figure 27.

$$\tilde{v}_0(t+1) = V\left(Q^{-1}\left(\tilde{q}_0(t+1)\right)\right)$$

Figure 27. Equation. Density-based algorithm step 2—advisory speed recommendation 2.

3. If $\Delta v(t) = |\tilde{v}_0(t+1) - \tilde{v}_0(t)| > \Delta v_{thr}$, then the equation shown in figure 28 is followed.

$$\tilde{v}_0(t+1) = \begin{cases} \tilde{v}_0(t) + \Delta v_{thr}, & \tilde{v}_0(t+1) > \tilde{v}_0(t) \\ \tilde{v}_0(t) - \Delta v_{thr}, & \tilde{v}_0(t+1) \le \tilde{v}_0(t) \end{cases}$$

Figure 28. Equation. Density-based algorithm step 3—advisory speed recommendation 1.

Let $v_{min} \le \tilde{v}_0(t+1) \le v_f$, for example, as shown in in figure 29.

$$\tilde{v}_0(t+1) = \max\left\{\min\left\{\tilde{v}_0(t+1), v_f\right\}, v_{min}\right\}$$

Figure 29. Equation. Density-based algorithm step 3—advisory speed recommendation 2.

Also the target flow rate is set, as shown in figure 30.

$$\tilde{q}_0(t+1) = Q\left(V^{-1}\left(\tilde{v}_0(t+1)\right)\right)$$

Figure 30. Equation. Density-based algorithm step 3—target flow rate.

4. If $t < T$, $t = t + 1$, then go back to step 2. Otherwise stop the iterations.

With the settings in step 2, the algorithm attempts to ensure that bottleneck flow rates approach bottleneck capacities. When the bottleneck is active, the algorithm reduces vehicular throughput from the speed harmonization zone. Alternatively, if the bottleneck is not active, the algorithm increases maximum throughput in the speed harmonization zone, allowing more vehicles to traverse the bottleneck. Moreover, α is introduced to smooth target speeds and flows in the speed harmonization zone. The value of α ranges between 0 and 1.

Testing (Part 1: INTEGRATION© Platform)

Calibration

Calibration of the INTEGRATION© software entailed two efforts: calibrating roadway supply parameters and calibrating traffic demand. Basic input files for INTEGRATION© include the network files and traffic demand file. Network files describe the network-wide topologic attributes and roadway features. The traffic demand file contains a time-varying origin-destination (OD) demand. Network files were converted from a shape file using the PYTHON™ program developed in an ArcGIS® environment.(9) Roadway attributes such as number of lanes, segment lengths, and speed limits were imported into INTEGRATION© from the shape file.

Traffic demands for the individual model years were estimated using the maximum likelihood synthetic OD estimation software, QueensOD©.(10) QueensOD© estimated the maximum likelihood OD table in order to replicate empirically observed link flows. The numerical solution begins by building a minimum path tree and performing an all-or-nothing traffic assignment of the seed matrix. A relative or absolute link flow error is computed depending on user input. Using the link-flow errors, OD adjustment factors are computed and used to modify the OD seed matrix. Adjustment of the OD matrix continues until one of two criteria are met: namely the change in OD error reaches a user-specified minimum or the number of iterations criterion is met. To estimate the traffic demand file, traffic count data from the trailers were used.

Final comparisons between observed counts and speeds suggest the following:

- Simulated speeds differed significantly from field-measured speeds.
- Simulated traffic counts were consistent with the field measurements.
- Simulated congestion temporally lagged behind field observations at some locations, but trends were consistent.
- End-of-corridor congestion was not captured because the downstream bottleneck was not modeled. Ideally, the network should have been extended to capture spillback from downstream bottlenecks.
- Simulated trajectories seemed to be consistent with the field observations.

Analysis

The proposed density-based algorithm was simulated using the calibrated INTEGRATION© software. Advisory speed recommendations were provided to CAVs entering I-66 from the

Route 7 on-ramp every 30 min. Table 2 shows the speed harmonization algorithm settings. Simulation results across the entire 6-h simulation are summarized in table 3. For 60 random seed replications, the scenario of three abreast CAVs was compared to baseline conditions (non-speed-controlled vehicles), with individual results recorded once every 30 min. Results demonstrate that the three CAVs had minimal impact on overall traffic conditions and minor savings in hydrocarbons (HC), carbon monoxide (CO), and nitrogen oxides (NOx) emissions. Specifically, *t*-test *p*-values for total travel delay, bottleneck discharge flow rate, fuel consumption, and carbon dioxide (CO_2) emissions were all much greater than 0.05. Thus, measures of effectiveness (MOEs) were not significantly different before and after applying the speed harmonization algorithm when only three abreast CAVs were controlled.

Table 2. Speed harmonization algorithm settings.

Parameter	Value
Target flow rate	5,100 vehicle/h
Target density	23.7 vehicle/mi/lane (14.7 vehicle/km/lane)
Maximum speed change	5 mi/h (8 km/h)
Minimum advisory speed recommendation	5 mi/h (8 km/h)
Update interval	30 s
Start time	1,200 s
End time	18,000 s
Coefficient of bottleneck capacity	0.6
Smoothing factor	0.5

Table 3. Density-based algorithm simulation results in INTEGRATION© with limited research vehicles.

Condition	TD	Fuel	HC	CO	NOx	CO_2	Flow at Bottleneck
Base	60.83 s/km	24.54 g/km	25,355.26 g/km	0.1193 g/km	0.568 g/km	14.500 g/km	2,996 vehicle/h
Speed harmonization	60.88 s/km	24.58 g/km	25,323.12 g/km	0.1187 g/km	0.564 g/km	14.401 g/km	2,998 vehicle/h
Difference (percent)	0.08	0.15	-0.13	-0.12	-0.59	-0.69	0.07
p-value (*t*-test)	0.9177	0.1947	0.0000	0.0000	0.0647	0.5278	0.8414

1 s/km = 1.61 s/mi
1 g/km = 0.057 oz/mi

Figure 31 compares CAV trajectories with and without the speed harmonization algorithm. The algorithm's influence indicates that if more CAVs were introduced into the network, traffic conditions downstream of the bottleneck would be improved.

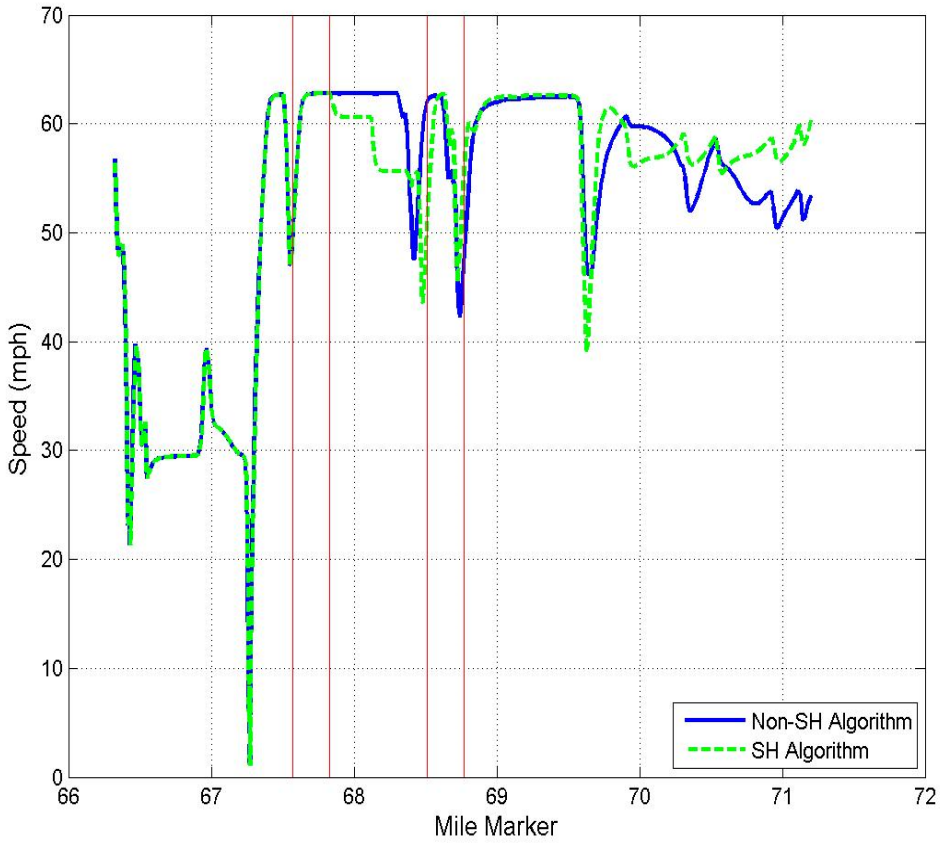

1 mi/h = 1.61 km/h

Figure 31. Graph. Vehicle trajectories before and after applying the density-based algorithm in INTEGRATION©.

Testing (Part 2: VISSIM® Platform)

Calibration

VISSIM® model calibration was conducted by a stochastic experimental design approach based on Latin hypercube sampling (LHS).(11) The LHS method was used to reduce the number of combinations to a sensible level while still reasonably covering the entire parameter surface. From several relevant calibration efforts performed in the past, it has been empirically observed that when the total number of calibration parameters is close to 10, approximately 500 to 1,000 LHS samples produce 1 or 2 optimal solutions.

The adopted performance measures included speed and traffic counts. To determine the quality of model calibration, performance measures obtained from field-deployed sensors were adjusted by the log transformation method (LTM). LTM is widely applied in practice where data are skewed, contain a significant number of outliers, or have unequal variations (e.g., travel time and traffic volumes).

In addition to several critical lane-changing model parameters, the VISSIM® Wiedemann-99 model was the primary target of calibration. Initial parameter ranges were set up as symmetric to

each side of the default value. Some parameter ranges were based on the project team's engineering judgment. Initial ranges for car-following and lane-changing parameters were obtained from prior research. Input volumes for VISSIM® were treated as calibration parameters to be adjusted. For the two target sections, preliminary calibration efforts from initial OD matrices produced significant discrepancies in field-observed travel times. This was mainly because initial OD matrices were estimated using older datasets from 2006, which did not reflect current traffic conditions. To overcome this, the OD matrices were converted to 30-min-interval input volumes for VISSIM®. Each 30-min interval volume was then added to the set of parameters to be calibrated.

LHS generated 500 initial parameter sets, and each set was simulated 5 times. RMSE values were computed by comparing average speeds and counts from simulation to those from field data. The best set (i.e., producing the lowest RMSE) was chosen by inspection and was used as the base parameter in creating two subsequent groups having 50 parameter sets each. Again after five simulations of each parameter set, the most promising set was chosen by inspection. Finally, the selected parameter set was fine-tuned to match field data.

With the final candidate parameter set demonstrating the lowest fitness value based on RMSE, fine-tuning efforts were conducted to obtain acceptable calibration results. The calibrated VISSIM® model matched the field data very well.

Analysis

The density-based algorithm was examined in the case of three CAVs and for a variety of market penetration rates through VISSIM®. However, it is important to note that due to the macroscopic nature of this simulation, it was not completely reflective of field test conditions. The CAVs received advisory speeds from the speed harmonization algorithm. They also received instructions to avoid lane changes and to keep moving parallel with adjacent CAVs. CAVs were dispatched every 30 min from the Route 7 on-ramp onto I-66 eastbound.

It was challenging to clearly observe impacts from the simulation results because only three CAVs were used. At the moment when CAVs were actually deployed, only a few temporary changes were observed, as shown in table 4 and table 5.

Table 4. Operational MOEs in VISSIM® (three-car case).

Average Travel Time (min)		Average Speed (mi/h)		Throughput (1,000 vehicle/h)	
Base	**Three Cars**	**Base**	**Three Cars**	**Base**	**Three Cars**
4.6	4.6	17.2	16.4	21.2	20.7

1 mi/h = 1.61 km/h

Table 5. Safety surrogate MOEs in VISSIM® (three-car case).

Number of Lane Changes		Number of Stops	
Base	**Three Cars**	**Base**	**Three Cars**
702.0	660.2	2,513.0	2,449.0

Operational performance of the density-based algorithm was also captured at the 10, 25, and 50 percent market penetration rates compared to the base case over 3 days. Results are shown in table 6 through table 8. The change in total distance appears insignificant, and each OD pair carrying a fixed traffic volume for each date consisted of a single route. This implies the total number of vehicles passing through the network was almost identical. Unlike total distance, the simulation showed that TTT was significantly affected. Given the insignificant changes in total distance, travel time reductions (up to 4 percent) suggest that the algorithm mitigated traffic congestion in simulation.

Table 6. Travel times at various market penetration rates in VISSIM®.

Metric	Base	10 Percent	25 Percent	50 Percent
Travel time (min)	4.6	4.6	4.5	4.4
Difference versus base case (percent)	—	0.9	-1.3	-2.5

— Indicates that no comparison was made.

Table 7. Speeds at various market penetration rates in VISSIM®.

Metric	Base	10 Percent	25 Percent	50 Percent
Speed (mi/h)	10.7	10.7	10.7	10.6
Difference versus base case (percent)	—	0.0	0.0	0.1

— Indicates that no comparison was made.

Table 8. Throughput at various market penetration rates in VISSIM®.

Metric	Base	10 Percent	25 Percent	50 Percent
Throughput (1,000 vehicle/h)	18.5	19.8	20.3	20.7
Difference versus base case (percent)	—	6.9	9.6	11.9

— Indicates that no comparison was made.

Impacts of the simulation were further examined by reviewing surrogate safety measures (i.e., number of stops, number of lane changes, and cumulative speed difference). Results are shown in table 9 through table 11. The algorithm appears to significantly reduce the number of stops, particularly in the critical upstream segments. Additionally, the total number of lane changes on these segments increased. Given the mobility improvement on those segments, such changes in stops and lane changing suggest the algorithm improved traffic flow. Cumulative speed difference exhibited little change throughout all segments.

Table 9. Stops at various market penetration rates in VISSIM®.

Metric	Base	10 Percent	25 Percent	50 Percent
Number of stops	3,759.1	3,868.5	3,773.4	3,753.8
Difference versus base case (percent)	—	2.9	0.4	-0.1

— Indicates that no comparison was made.

Table 10. Lane changes at various market penetration rates in VISSIM®.

Metric	Base	10 Percent	25 Percent	50 Percent
Number of lane changes	704.9	768.6	810.0	585.5
Difference versus base case (percent)	—	9.0	14.9	21.8

— Indicates that no comparison was made.

Table 11. Cumulative speed difference at various market penetration rates in VISSIM®.

Metric	Base	10 Percent	25 Percent	50 Percent
Cumulative speed difference	1,675.3	1,739.7	1,772.4	1,782.5
Difference versus base case (percent)	—	3.8	5.8	6.4

— Indicates that no comparison was made.

CHAPTER 2. FIELD EXPERIMENTS

Field runs were performed using three CAVs with V2I-based speed harmonization capability, which were used to control traffic streams on sections of I-66 in Northern Virginia during periods of increasing congestion. By communicating to roadside equipment capable of accessing real-time roadway speeds and volume, a surrogate traffic management center at the Turner-Fairbank Highway Research Center (TFHRC) was used to calculate variable speed recommendations. These speeds were transmitted to the CAVs. These field runs tested the impacts of optimized variable speed targets, including changes to speed oscillations, travel time, and traffic throughput. A total of 19 runs were conducted in June 2014, July 2014, September 2015, and October 2015. This chapter reviews the setup, methodology, results, and analysis of the field testing conducted on the selected test corridor.

VEHICLE AND INFRASTRUCTURE SETUP

Vehicles

To execute the speed harmonization experiment on a microscopic scale but in active traffic on a congested freeway, the project team built a fleet of three CAVs.[(12)] These vehicles were modified such that longitudinal control (e.g., vehicle set speed and gap) was accomplished from a central control center using V2I communication over a cellular digital network. Commands were sent over a V2I connection into an onboard computer. Commands generated by the onboard computer were communicated over a controller area network bus to the original equipment manufacturer (OEM)-supplied ACC system. This experimental equipment allowed remote control over the longitudinal speed of individual vehicles. The modified vehicles were operated by drivers in a mode where safety was enhanced, as the OEM-supplied ACC maintained a minimum headway (1.1 s). Vehicle operators had complete control over the latitudinal control (steering) and could override V2I recommendations using the brake and accelerator pedals. The intent for the vehicle fleet was that speed recommendations based on measurements from a variety of locations on the roadway could be used with algorithms selected for laboratory testing. These allowed algorithms were implemented in the laboratory to be used for live freeway testing in a living laboratory environment.[(13)]

Infrastructure

Input to the CAVs was based on corridor traffic speed measurement processing, as shown in figure 32. The project team developed a connected mobile traffic sensing (CMTS) trailer, including an RTMS measuring 15-s averaged speeds, volumes, and occupancies. These CMTS trailers were deployed along the roadway corridor. Measurements were relayed in real time to a central computer. The computer used this data to calculate recommendations to be sent to the CAVs. Figure 33 shows the CMTS trailer locations along I-66 as labeled trailers 4 through 6 containing the RTMSs used as sensors. Input to the CAVs was therefore based on macroscopic measures obtained along the test corridor.

©2016 Google® (Modifications: See Acknowldgements).

Figure 32. Map. Field experiment map of system integration.[14]

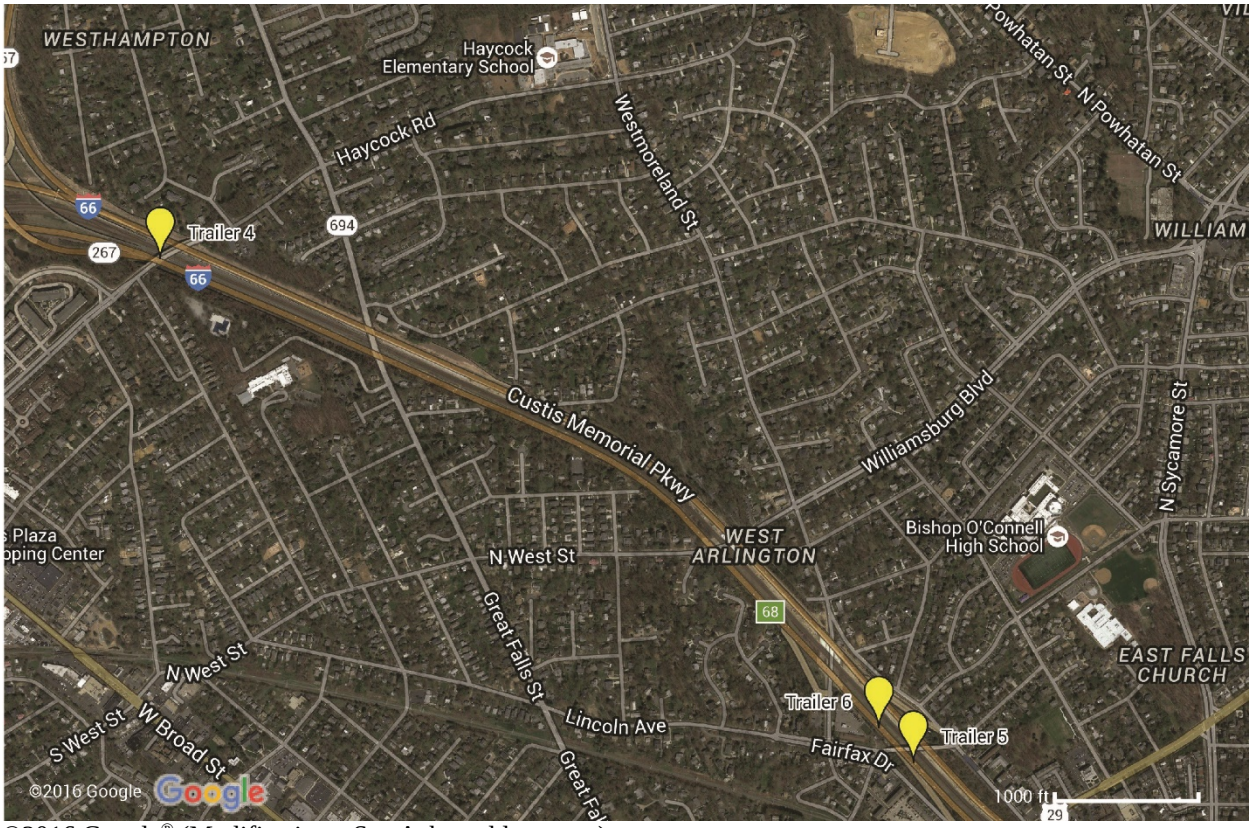

©2016 Google® (Modifications: See Acknowldgements).

Figure 33. Map. Test segment and trailer locations.[15]

METHODOLOGY

The experiment hypothesized that by controlling traffic flow speeds in a congested region, traffic flows could be smoothed and that smoothing may provide operational and safety benefits. The experiment was performed on I-66 using the following:

- Three CAVs equipped with V2I to control the traffic speed.
- A lead probe vehicle placed in the traffic stream approximately 328.08 ft (100 m) ahead of the CAVs to measure traffic flows downstream of the speed control effort.
- Two probe vehicles approximately 164.04 ft (50 m) behind the CAVs to measure traffic flows upstream of the speed control effort.

Each vehicle had an onboard computer to record and communicate vehicle state (e.g., location, speed, acceleration, etc.) at a 10-Hz frequency to the laboratory in real time. The experiment was microscopic in nature, as the traffic flow monitoring was localized by probe vehicles to several hundred feet (meters) around the CAVs.

Mechanics of the experiment called for time periods in which the freeway would transition into congested conditions. Real-time speed data from the RTMSs were used to determine when to initiate the experiment. The experimenter at TFHRC monitored speeds recorded by the RTMSs. The experiment was initiated when speed measurements at the ends of the test corridor met threshold requirements. In this study, threshold requirements had an upstream speed recommendation approximately equal to the 60 mi/h (96.56 km/h) (i.e., free-flow speed) and a downstream speed approximately 10 mi/h (16.1 km/h) below the upstream speed. The six vehicles used in the experiment were staged near the test corridor's on-ramp so as to be launched into the traffic stream at the appropriate time.

The leading probe, which was used to measure existing traffic conditions, was sent down the roadway first. Its driver was instructed to travel in the center lane (out of three) at prevailing typical speeds. Figure 34 illustrates the experimental fleet configuration when vehicles were fully deployed on the freeway. It was assumed that on a microscopic traffic flow level, the leading probe trajectory represented typical traffic flow behavior.

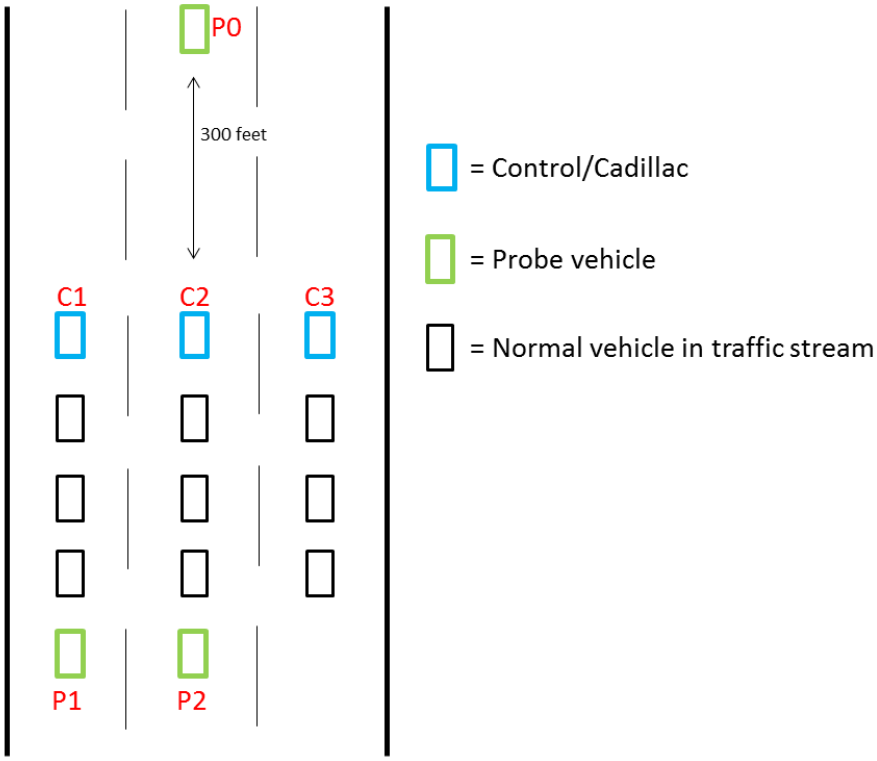

Figure 34. Illustration. Research and probe vehicle placement.

Next, the three CAVs entered the freeway as a group. They traveled at prevailing traffic speeds while adopting a parallel formation across the three lanes. The CAVs were switched into automated longitudinal control mode (speed and braking) upon entering the control section. The control section start was demarcated by location of the upstream CMTS trailer (trailer 4). The control section end was demarcated by the furthest downstream CMTS trailer (trailer 5). Drivers of the CAVs were instructed to remain in the lane assigned to each. CAV speeds were controlled from a central computer, which generated a longitudinal (along the roadway) speed profile as a function of position along the roadway. Automation within the vehicles downloaded speed recommendations every 2 s and directed the ACC to adjust speed accordingly. These vehicles traversed the control section under the automated speed recommendation algorithm executed by the central computer. At the end of the control section, the CAVs stopped downloading speed recommendations and once again mimicked the prevailing typical speeds.

The two following probes entered the freeway last. They positioned themselves in the two leftmost lanes (see figure 34) some distance 164.04 to 328.08 ft (50 to 100 m) behind the CAVs. Probe vehicle drivers were instructed to travel at prevailing typical speeds. Trajectory characteristics of the following probes, as recorded and relayed to the laboratory in real time, were the surrogate for measuring traffic impacts resulting from speed harmonization. Probe vehicle trajectory statistics were used to represent the results on a microscopic scale of the speed harmonization experiment.

The test corridor for the experiment consisted of a control section followed by a section of roadway where no control was applied. This allowed for comparing mobility benefits on nearby and similar sections of roadway, with and without speed harmonization impacts.

The algorithm created to produce speed recommendations was influenced by but differed from the work done in microscopic simulation for this corridor.[13,16] During pilot testing, the initial algorithm implementation reduced speeds too rapidly before following probes entered the congested test corridor. The three CAVs (travelling at near free-flow speeds of 50–60 mi/h (80.5–96.6 km/h)) received reduced-speed recommendations from the algorithm and adopted it as their set speed; however, the initial algorithm, upon detecting congestion in the test corridor, recommended a speed of 25 mi/h (40.2 km/h), the lowest possible set speed under cruise control. With surrounding vehicles travelling at free flow speeds, this created highly unsafe conditions. Therefore, a simplified speed-space relationship was developed. This approximated the complex relationships developed by past speed harmonization simulation efforts.

In these field experiment runs, the speed recommendation $s(x,t)$ was a linear function of space (x) depending upon temporal (t) speed measurements from the roadside RTMSs as seen in figure 35 as follows:

$$s(x,t) = \left(\frac{s_n(t) - s_m(t)}{\Delta x_{nm}}\right)x + s_n(t)$$

Figure 35. Equation. Field experiment speed recommendation.

Where:

$s_n(t)$ = Speed measurement at trailer n at time t.
$s_m(t)$ = Speed measurement at trailer m at time t.
Δx_{nm} = Distance between trailers n and m.

This simplified speed-space relationship was used to test both performance of the CAVs and impacts on existing traffic flow. The speed recommendation has a floor value of 25 mi/h (40.2 km/h).

ANALYSIS

Data from the experimental probe and CAVs were used to answer the following basic questions:

1. Does speed control from the simple algorithm result in appropriate behavior in terms of speed as a function of location along the corridor?

2. Are statistics from the leading and following probes significantly different?

3. In characterizing the change in statistics between leading and following probes, do there appear to be significant potential benefits?

Vehicle Control

Speed recommendations for the CAVs were generated every 2 s using the linear speed harmonization algorithm based on speed values measured by RTMSs. There was a minimum value of 25 mi/h (40.2 km/h) enforced on the recommendations.

Figure 36 illustrates an example of CAV performance in this experiment. In the figure, CAV trajectory is plotted as a solid line, and the speed recommendations are plotted as points. CAVs generally followed the recommendations in all cases. The exceptions, exemplified near mile marker 68.25, occurred when CAVs were impeded by existing traffic. This is likely due to the use of radar to sense downstream vehicles, which would then set a minimum headway of 1.1 s. When the headway decreased past this threshold, the vehicular OEM systems performed braking maneuvers.

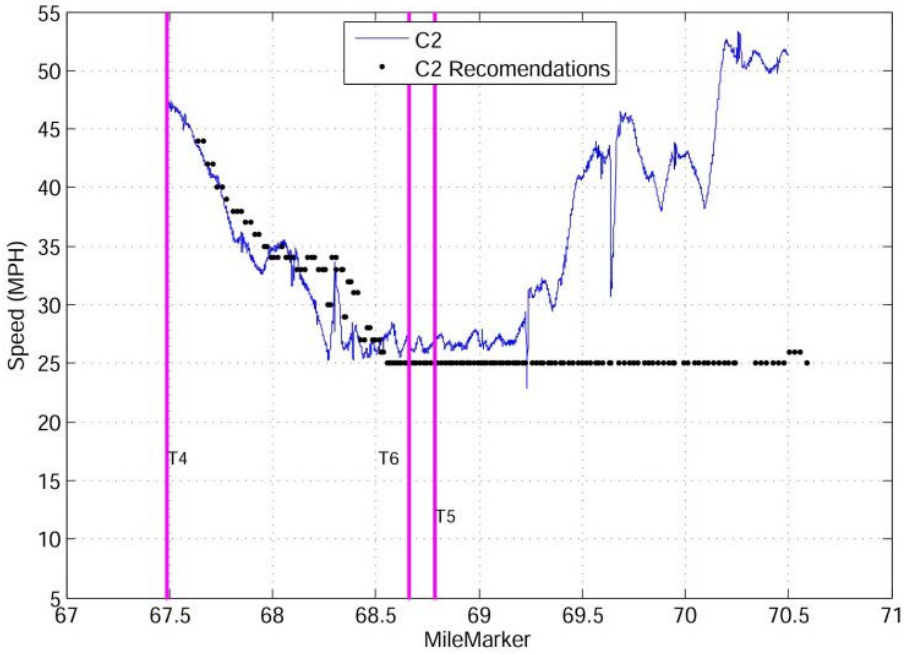

1mi/h = 1.61 km/h

Figure 36. Graph. Control vehicle trajectories and recommendations.

The conclusion, with regard to the first question in the previous list, is that CAVs operating in traffic can be expected to operate at recommended speeds (provided that speed is at or below existing traffic speed) with a small time delay. This affirmation of a positive answer to question 1 is a similar result to other CACC tests without a closed loop controller.[17]

Probe Vehicles/Sensors

The probe vehicles were intended to act as high-resolution sensors of traffic conditions over a small region surrounding the CAVs in an effort to answer questions 2 and 3. Figure 37 shows the probe and CAV speed trajectories as a function of time. Figure 38 shows the speed trajectories as a function of mile marker. The probe and CAVs were released onto the roadway at slightly different times. As a result, the temporal and spatial relationships between experimental vehicles

were not equivalent. It was asserted for this experiment that the recurring traffic congestion on this segment of roadway set up a stable but oscillatory structure along the roadway. In order to observe this behavior, the trajectories are best compared with space as the independent variable, as shown in figure 38.

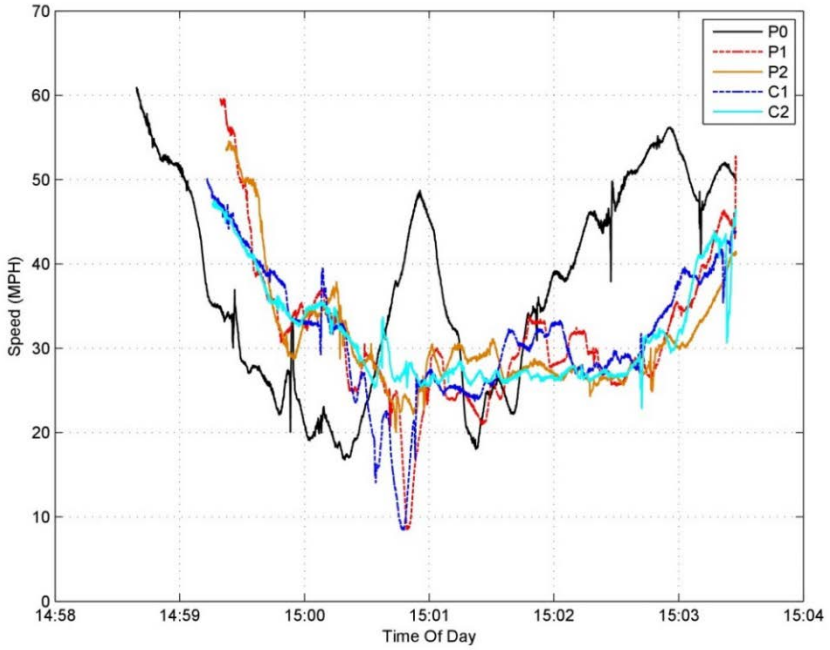

1mi/h = 1.61 km/h

Figure 37. Graph. Temporal speed trajectories.

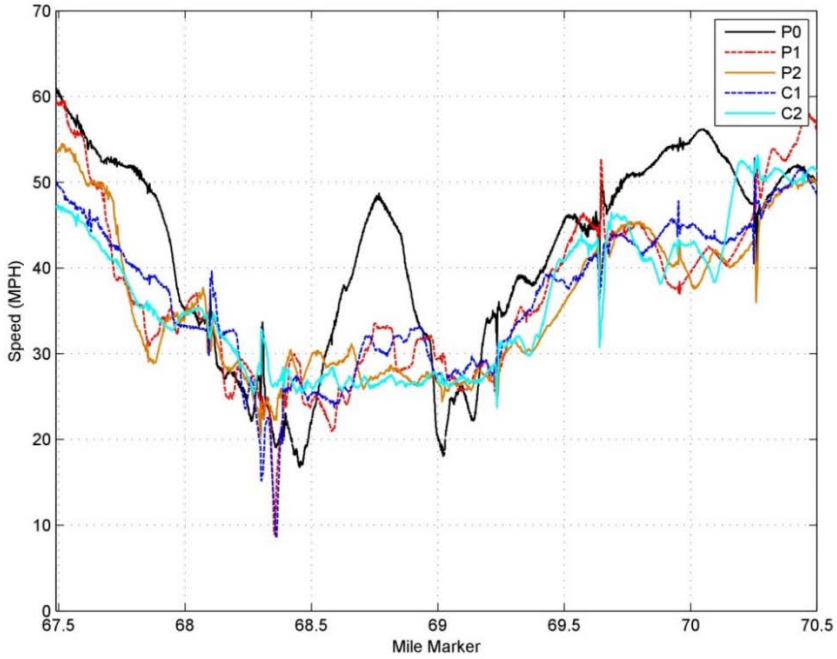

1mi/h = 1.61 km/h

Figure 38. Graph. Spatial speed trajectories.

Trajectories of the probe and CAVs were impacted by both the surrounding traffic and by speed control enforced by the CAVs. CAV deviations from the programmed speed profile were primarily caused by slowing in response to exiting traffic. The resulting CAV speed profile had a large-scale spatial trend associated with control and congestion around which there were stochastic fluctuations. For example, the overall trend can be represented by a smooth version of the resulting CAV speed profile (see figure 39).

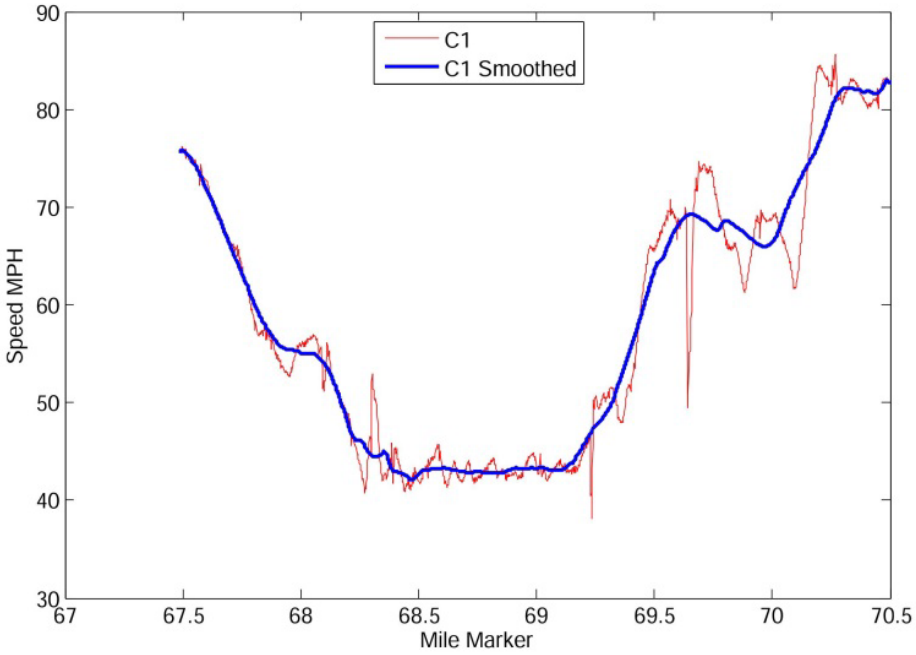

1mi/h = 1.61 km/h

Figure 39. Graph. Control speed trajectory and smoothed profile.

In order to characterize the trajectories, changes in the stochastic traffic flow component before and after probe vehicle passage were considered. To examine the stationary statistics of the trajectories, the overall trend was removed from the probe vehicle trajectories. The detrended trajectories are shown in figure 40.

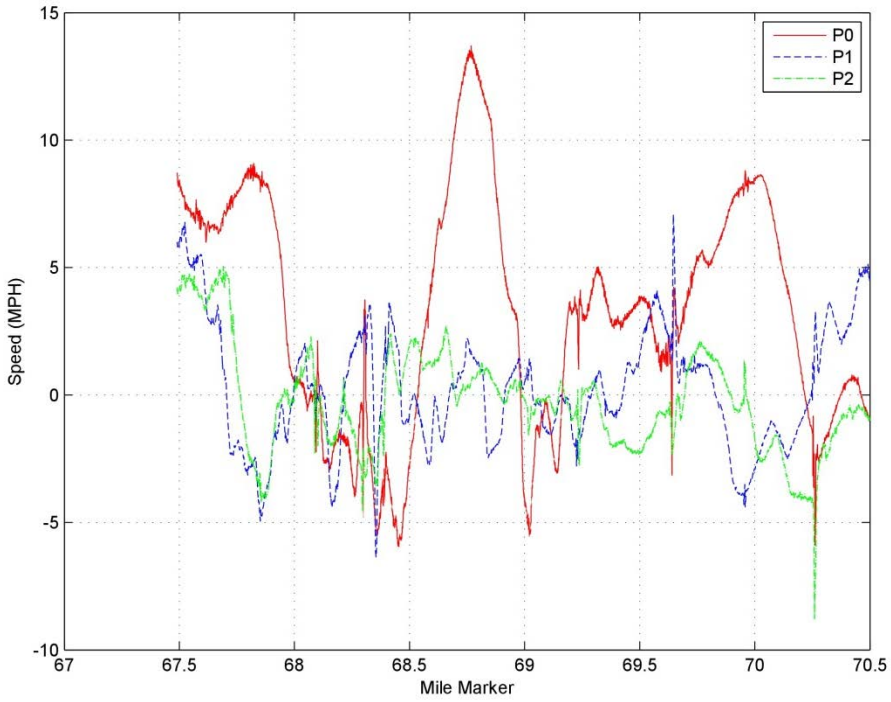

1mi/h = 1.61 km/h

Figure 40. Graph. Detrended probe vehicle speed trajectories.

The probability density function (PDF) for a following probe trajectory is shown in figure 41, and the detrended PDF is shown in figure 42. The detrended data were approximately second-order stationary (constant temporal mean and variance for each probe) and thus could be examined using typical time series techniques in order to address question 2.

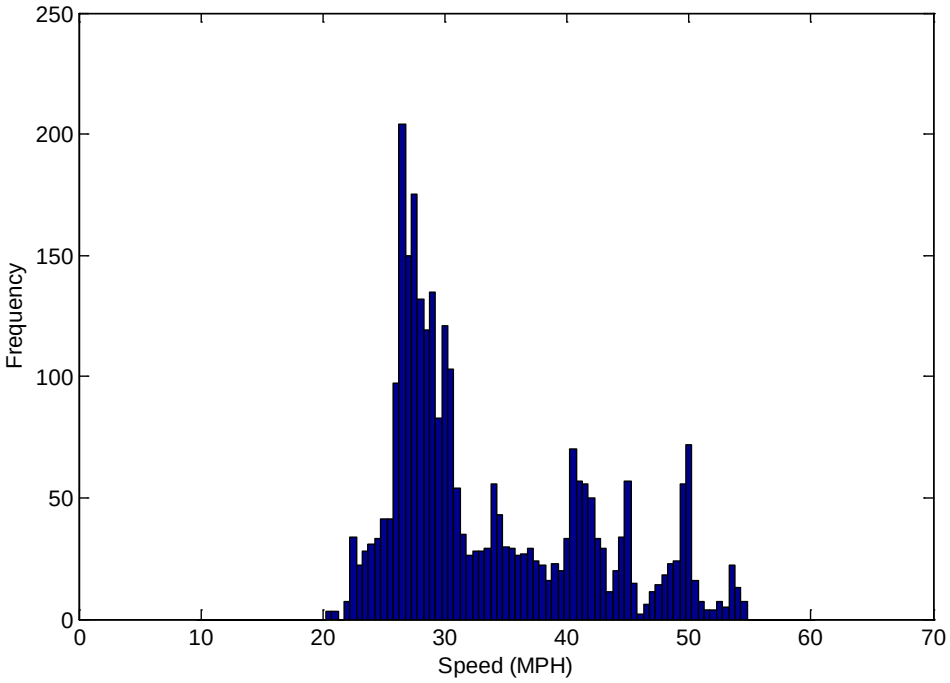

1mi/h = 1.61 km/h

Figure 41. Graph. PDF of raw data following probe speed trajectory.

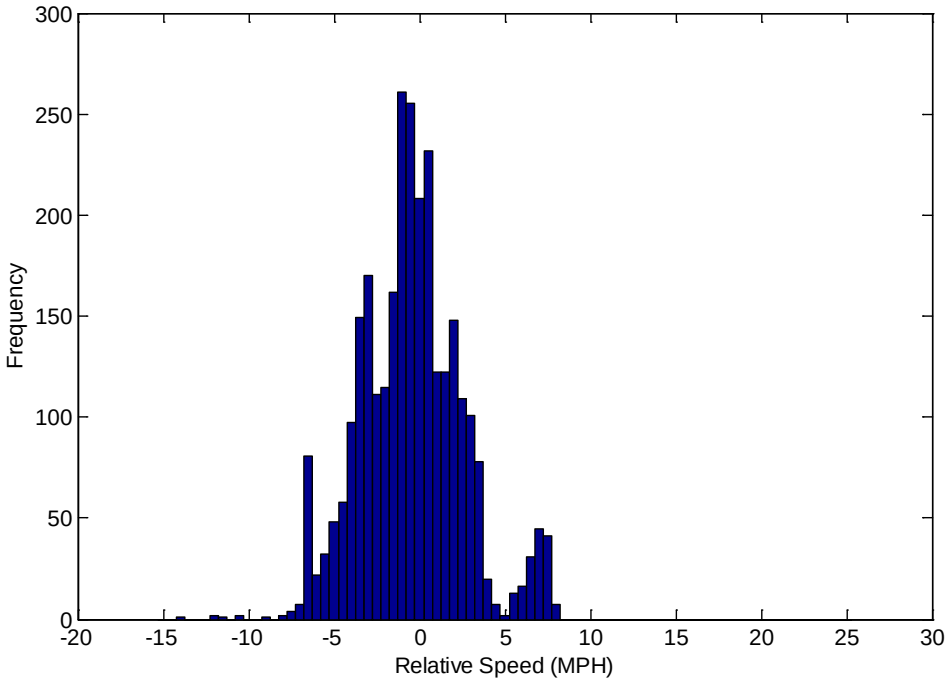

1mi/h = 1.61 km/h

Figure 42. Graph. PDF of detrended following probe speed trajectory.

The impact of speed harmonization could be observed in both the time and frequency domains. In the time domain, a stochastic process could be characterized by its PDF. In this study, the

process histograms were used as a surrogate for the PDF. The PDF of the leading probe detrended speed trajectory, which characterizes traffic flow before speed harmonization is applied, is shown in figure 43. The PDFs clearly indicate different processes were measured before and after the control. The PDF shapes imply that the resulting traffic flow had lesser variability and was distributed about a single mode. In the time domain, it can thus be concluded that speed harmonization did indeed change the statistics and nature of the traffic flow.

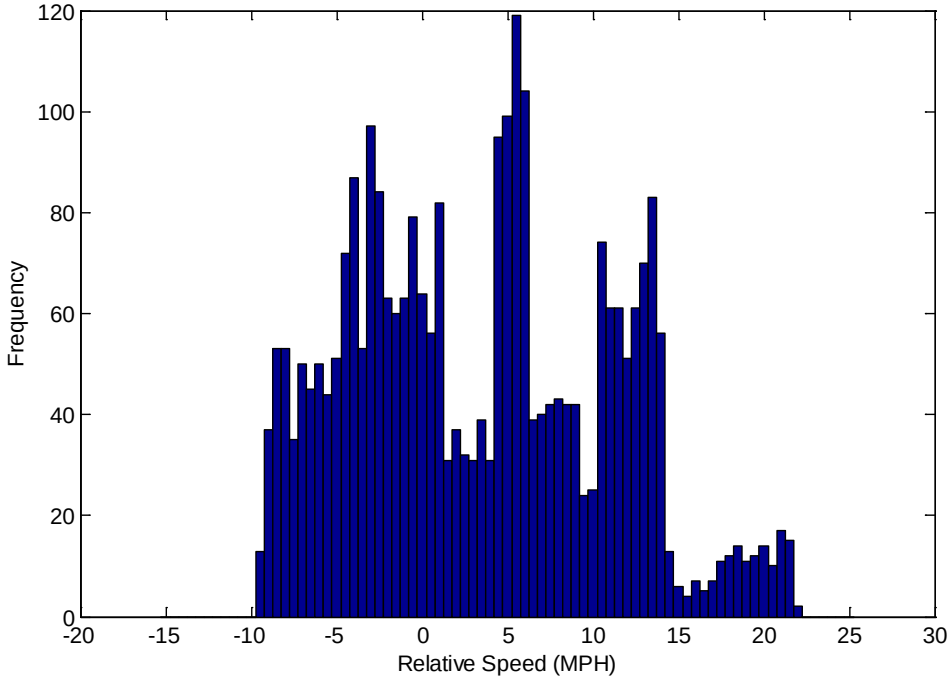

Figure 43. Graph. PDF of detrended leading probe speed trajectory.

Temporal characteristics of a stationary stochastic process are often characterized by the frequency content of the measured signals. In this study, the independent variable of distance along the roadway (i.e., mile marker) was treated as an ordered sampling base in the same way that time was used in time-series applications. The detrended speed trajectories were Fourier transformed (i.e., using a padded fast Fourier transform), and the power spectral density (PSD) was estimated.[(18)] PSD describes the amount of signal energy found at each frequency in the signal. For example, a signal consisting of a pure sinusoid will appear as a single peak in the PSD. A large PSD indicates oscillatory behavior. Figure 44 through figure 47 present the PSDs for the leading (P0) and following (P1 and P2) detrended trajectories on four separate field runs. In each case, the PSD for the leading probe vehicle shows large peaks. This indicates a significant oscillatory behavior in the traffic flow, which occurs on the order of one to two cycles per mile. PSDs for the following probes did not have these strong peaks at low frequencies.

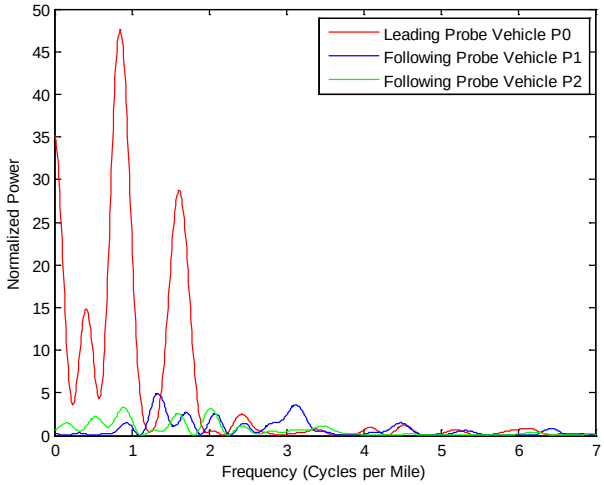

Figure 44. Graph. PSDs of detrended speed trajectories of the probe vehicles on July 8, 2014.

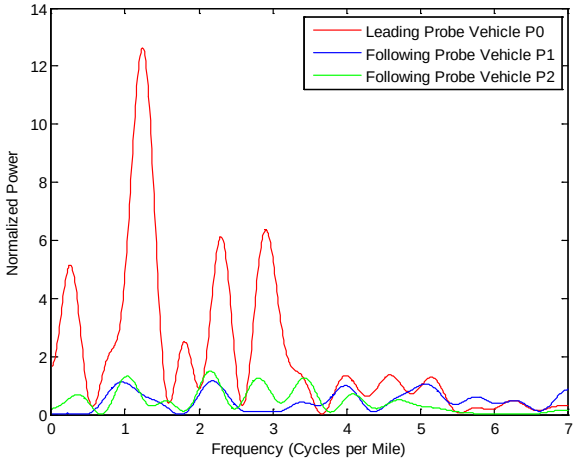

Figure 45. Graph. PSDs of detrended speed trajectories of the probe vehicles on September 29, 2015.

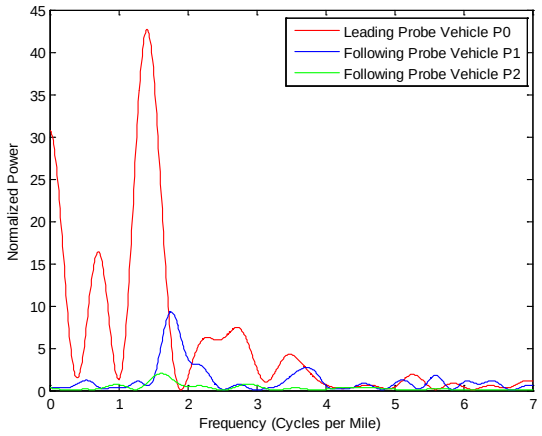

Figure 46. Graph. PSDs of detrended speed trajectories of the probe vehicles on October 15, 2015.

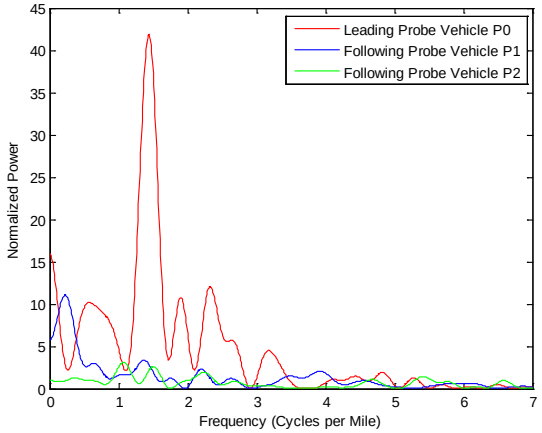

Figure 47. Graph. PSDs of detrended speed trajectories of the probe vehicles on October 21, 2015.

The PSD trends imply that speed harmonization acted effectively as a low-pass filter for speed fluctuation of the traffic stream. These PSD estimates indicate that the answer to question 2 is that traffic flow stream statistics were significantly different as a result of speed harmonization. The speed trajectories resulting from this control were indeed harmonized in the sense that measured oscillations in the traffic stream were dampened.

Potential Benefits

The answer to the third question regarding potential benefits has two aspects: first, are the impacts observed in some way beneficial, and, second, is there a disbenefit that offsets the possible benefits?

The reduction in oscillatory behavior has been shown to improve (reduce) fuel consumption in past work.[19] Results from this limited test indicate that for cases where the traffic stream was not broken down (e.g., became purely stop and go), there was a significant reduction in oscillatory traffic stream speed, implying a fuel consumption benefit.

Oscillations and large variability in traffic stream speed behavior have been associated with safety risks. This is often the underlying premise for applications such as queue warning.

On the disbenefit side of the equation, there is the potential for increasing segment travel times by applying speed harmonization. In this study, the following probes did not show a significant or consistent reduction in travel times compared to leading probe travel times, and thus the travel time disbenefit was not observed. That said, the experiment reported here was done on a microscopic traffic scale (though repeatedly), and these results are not guaranteed to materialize in a macroscopic measurement framework. This linkage of microscopic results to macroscopic outcomes for this application of CAVs has yet to be tested.

CHAPTER 3. CONCLUSIONS

This project implemented speed harmonization algorithms on an active freeway with recurring spatially structured congestion in simulation and field testing using a fleet of CAVs. Due to resource constraints, the field experiments could only deploy a maximum of three CAVs. Simulation results across three platforms (VISSIM®, INTEGRATION©, and Aimsun®) showed that the introduction of three CAVs, with a goal of harmonizing overall speeds, would not be beneficial on a real-world freeway.

The simulation results indicated that a field experiment with a limited volume of CAVs was unlikely to cause a significant negative impact on traffic. The field experiment demonstrated that CAVs, with automation in the form of modifications to the OEM-supplied ACC, can be used in automated longitudinal control mode to implement V2I-based speed harmonization. The impacts on the traffic stream were measured using probe vehicles leading and following the CAVs. Furthermore, this project demonstrated that traffic stream trajectories after speed harmonization reduced oscillatory behavior as characterized using the power spectral densities of the measurements. In addition, there was no disbenefit in terms of travel times between the probe vehicles before and after speed harmonization.

ACKNOWLDGEMENTS

The original maps shown in figure 32 and figure 33 are the copyright property of Google Maps® and can be accessed from http://maps.google.com. The maps contain overlays of markers, shapes, and arrows depicting CMTS trailer locations; vehicles, CMTS trailers, and the server at the Saxton lab; and the communication between these items, respectively. These map overlays were developed as a result of this research project.

REFERENCES

1. Talebpour, A., Mahmassani, H.S., and Hamdar, S.H. (2013). "Speed Harmonization: Evaluation of Effectiveness Under Congested Conditions," *Transportation Research Record 2391*, 69–79, Transportation Research Board, Washington, DC.

2. Lu, X.Y., Shladover, S.E., Jawad, I., Jagannathan, R., and Phillips, T.H. (2015). *A Novel Speed-Measurement Based Variable Speed Limit/Advisory Algorithm for a Freeway Corridor with Multiple Bottlenecks*, 94th Transportation Research Board Annual Conference, Washington, DC.

3. Eisele, B., Schrank, D., and Lomax, T. (2011). *2011 Congested Corridors Report*, Texas Transportation Institute, College Station, TX. Obtained from: http://tti.tamu.edu/documents/corridors-report-2011.pdf. Site last accessed October 20, 2014.

4. Google Maps®. (2016). *Geographic scope of the study area and typical traffic situation in afternoon peak hours*. Generated by: Kelli Raboy via Google Maps® online. Obtained from: https://www.google.com/maps/@38.8926484,-77.1691639,15z/data=!5m1!1e1. Generated January 19, 2016.

5. PTV Vissim®. (2011). *PTV Planung Transport Verkehr AG*, Version 5, Karlsruhe, Germany.

6. INTEGRATION©. (2005). *INTEGRATION*, Version 2.30, M. Van Aerde & Assoc., Ltd., Kingston, Canada.

7. Aimsun®. (2011). *Aimsun*, Version 7, TSS—Transport Simulation Systems, Barcelona, Spain.

8. Hellinga, B.R. and Van Aerde, M. (1998). "Estimating Dynamic O-D Demands for a Freeway Corridor Using Loop Detector Data," *Proceedings of the Canadian Society for Civil Engineering 1998 Annual Conference*, Volume IVb, 185–197, Halifax, NS, Canada.

9. ArcGIS®. (2102). *ArcGIS*, Version 10.1, Esri, Redlands, CA.

10. QueensOD©. (2010). *QueensOD*, Version 2.10, M. Aerde and Associates, Ltd., Kingston, Canada.

11. McKay, M.D., Beckman, R.J., and Conover, W.J. (1979). "A Comparison of Three Methods for Selecting Values of Input Variables in the Analysis of Output from a Computer Code," *Technometrics*, *21*(2), 239–245 (reprinted in 2000: *Technometrics*, *42*(1), 55–61).

12. Lochrane, T.W.P., Al-Deek, H., Dailey, D.J., and Bared, J. (2014). "Using a Living Laboratory to Support Transportation Research for a Freeway Work Zone," *Journal of Transportation Engineering*, *140*(7).

13. Lee, J., Dailey, D.J., Bared, J.G., and Park, B. (2013). *Simulation-Based Evaluations of Real-Time Variable Speed Limit for Freeway Recurring Traffic Congestion*, presented at the

Transportation Research Board 92d Annual Meeting Compendium of Papers, Washington, DC.

14. Google Maps®. (2016). *Field experiment map of system integration*. Generated by: Kelli Raboy via Google Maps® online. Obtained from: https://www.google.com/maps/@38.8962891,-77.170151,15z. Generated January 19, 2016.

15. Google Maps®. (2016). *Test segment and trailer locations*. Generated by: Kelli Raboy via Google Maps® online. Obtained from: https://www.google.com/maps/d/edit?mid=z9ibUIsfYaqM.kvEPSlnetVnY&usp=sharing. Generated January 19, 2016.

16. Lu, X.Y., Lee, J., Chen, D., Bared, J., Dailey, D.J., and Shladover, S.E. (2014). *Freeway Micro-Simulation Calibration: Case Study Using Aimsun and VISSIM with Detailed Field Data*, presented at the Transportation Research Board 93d Annual Meeting Compendium of Papers, Washington, DC.

17. Milanes, V., Shladover, S.E., Spring, J., Nowakowski, C., Kawazoe, H., and Nakamura, M. (2014). "Cooperative Adaptive Cruise Control in Real Traffic Situations," *IEEE Transactions on Intelligent Transportation Systems*, *15*, 296–305.

18. Bendat, J.S. and Piersol, A.G. (1980). *Engineering Applications of Correlation and Spectral Analysis*, Wiley, New York, NY.

19. Ahn, K., Rakha, H., Trani, A., and Van Aerde, M. (2001). "Estimating Vehicle Fuel Consumption and Emissions Based on Instantaneous Speed and Acceleration Levels," *Journal of Transportation Engineering*, *128*,182–190.

HRDO-20/03-16(WEB)E